


Review

# Tribocorrosion and Surface Protection Technology of Titanium Alloys: A Review

Yang Li <sup>1,\*</sup> , Zelong Zhou <sup>1</sup> and Yongyong He <sup>2,\*</sup>

<sup>1</sup> School of Nuclear Equipment and Nuclear Engineering, Yantai University, Yantai 264005, China; zhouzelong20000313@163.com

<sup>2</sup> State Key Laboratory of Tribology, Tsinghua University, Beijing 100084, China

\* Correspondence: metalytu@163.com (Y.L.); heyy@mail.tsinghua.edu.cn (Y.H.)

**Abstract:** Titanium alloy has the advantages of high specific strength, good corrosion resistance, and biocompatibility and is widely used in marine equipment, biomedicine, aerospace, and other fields. However, the application of titanium alloy in special working conditions shows some shortcomings, such as low hardness and poor wear resistance, which seriously affect the long life and safe and reliable service of the structural parts. Tribocorrosion has been one of the research hotspots in the field of tribology in recent years, and it is one of the essential factors affecting the application of passivated metal in corrosive environments. In this work, the characteristics of the marine and human environments and their critical tribological problems are analyzed, and the research connotation of tribocorrosion of titanium alloy is expounded. The research status of surface protection technology for titanium alloy in marine and biological environments is reviewed, and the development direction and trends in surface engineering of titanium alloy are prospected.

**Keywords:** titanium alloys; tribocorrosion; marine; plasma surface engineering

## 1. Introduction

Titanium alloy has the advantages of low density, high specific strength, good corrosion resistance, good heat resistance, low-temperature resistance, being non-magnetic, good impact resistance, and good welding performance [1–8]. It is widely used in aerospace, marine engineering, medical biology, and other fields [9–15]. In ship and marine engineering, titanium and titanium alloys have better seawater corrosion resistance than stainless steel and copper alloys [16–18]. They are widely used in ship hulls, sea pipelines, pumps, valves, seawater desalination devices, deep-sea detectors, offshore oil platforms, etc., known as ‘marine metals’ [19,20]. In addition to being corroded by seawater, titanium and titanium alloy structural materials are also subjected to mechanical effects such as friction/erosion, often leading to unpredictable sudden failure and causing huge losses. Therefore, studying their tribocorrosion behavior and mechanism is necessary.

Titanium alloy has developed into a primary material for high-end surgical implants with high specific strength, good biocompatibility, and mechanical compatibility [21–25]. In particular, additive manufacturing technology based on a digital model can form a personalized titanium alloy with a porous structure, which can effectively solve the problem of stress shielding between dense metal and human bone and is conducive to the growth of bone tissue [26–33]. Titanium alloy implants are more and more widely studied and applied. The global medical device market is expected to grow from nearly USD455 billion in 2021 to USD658 billion in 2028 due to increasing healthcare facilities, the elderly population, healthcare expenditures, and technological advances [34].

Tribocorrosion in the marine environment can cause damage to titanium alloy components, affecting their service life and safety [35–37]. The synergistic effect of friction and corrosion is mainly manifested as physical spalling and chemical corrosion on the



**Citation:** Li, Y.; Zhou, Z.; He, Y. Tribocorrosion and Surface Protection Technology of Titanium Alloys: A Review. *Materials* **2024**, *17*, 65. <https://doi.org/10.3390/ma17010065>

Academic Editor: Yong Sun

Received: 31 October 2023

Revised: 28 November 2023

Accepted: 13 December 2023

Published: 22 December 2023



**Copyright:** © 2023 by the authors. Licensee MDPI, Basel, Switzerland. This article is an open access article distributed under the terms and conditions of the Creative Commons Attribution (CC BY) license (<https://creativecommons.org/licenses/by/4.0/>).

surface of titanium alloy [38–40]. The physical spalling is mainly caused by the impact of seawater and the wear of particles. At the same time, chemical substances in seawater, such as oxidants, sulfides, and chlorides, will rapidly erode the surface of titanium alloys and accelerate their corrosion rate [41–44]. When physical exfoliation and chemical corrosion exist simultaneously, the synergistic effect of tribocorrosion will be formed, accelerating the damage to titanium alloy parts [45,46].

When titanium alloy is used as an implant material in a complex human environment, the implanted titanium alloy will be corroded by the surrounding body fluid, and the bone interface between the implant and the tooth will be worn [3,47–49]. Under the synergistic effect of tribocorrosion, the implanted titanium alloy will be damaged due to the decrease in fatigue, and the wear debris and corrosion products generated during the tribocorrosion process will lead to cell damage and cause inflammation, allergic reactions, and rashes, which will cause significant harm to health [50–54].

In summary, the prevention of tribocorrosion of titanium alloy in the human environment and marine environment is of great significance to ensure the safety of use, reduce maintenance costs, and prolong the service life of components. Various surface modification techniques have been widely used to improve tribocorrosion performance—for example, PVD, plasma spot oxidation, plasma chemical heat treatment, laser cladding, etc. Figure 1 shows the application scenarios of titanium alloys and some surface modification techniques and technical principles used to improve titanium alloys' friction and corrosion properties.

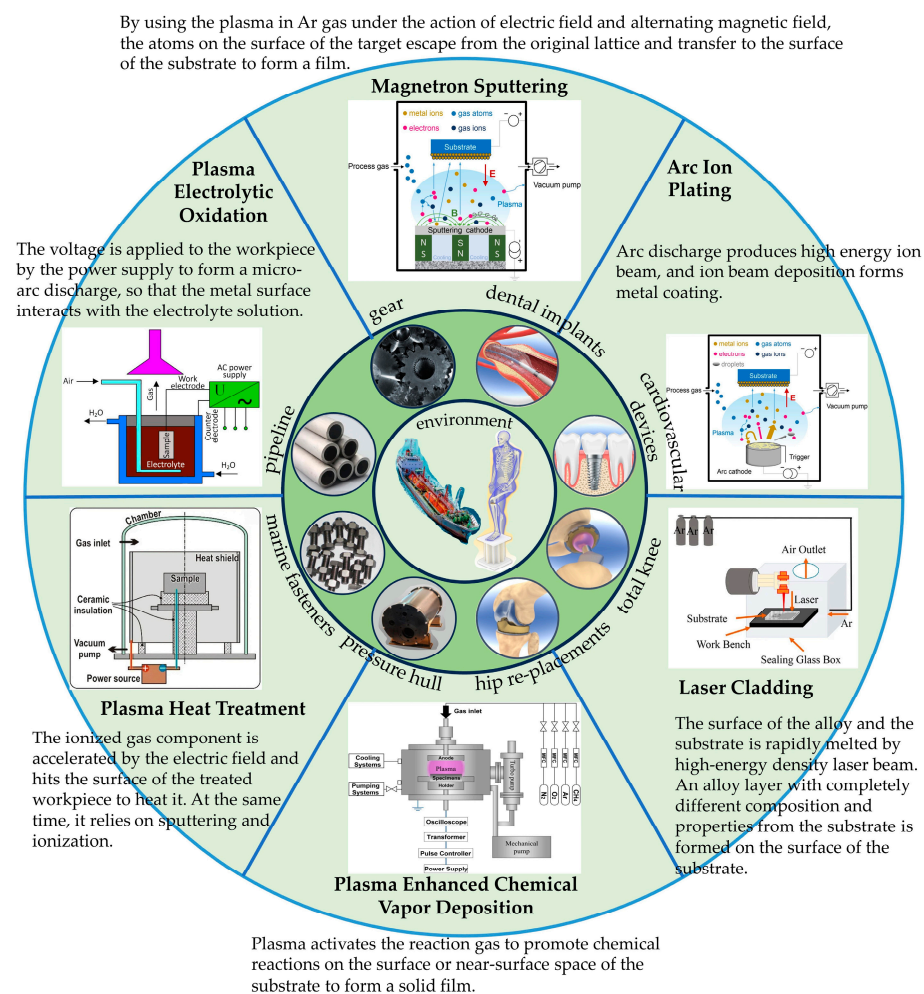


**Figure 1.** Titanium alloy application scenarios and surface modification techniques and principles for improving the tribocorrosion properties of titanium alloys [55–58].

With the continuous expansion of the application range of titanium alloy in marine engineering, biomedicine, and other fields, it is necessary to study the tribocorrosion problems of titanium alloy under special working conditions. Surface modification of titanium alloy can effectively improve its tribological properties in seawater environments and human body fluids, prolong its service life, and improve its reliability.

This paper reviews the research background of tribocorrosion of titanium alloys, focusing on the marine and human environments. Subsequently, various surface modification methods for improving the tribocorrosion properties of titanium alloys are introduced. Finally, the research on friction corrosion of titanium alloy is prospected.

## 2. Titanium Alloy and Its Classification and Properties

Titanium is an allotrope element with different crystal shapes. Titanium alloy has a hexagonal close-packed (hcp) crystal structure at room temperature, labeled as  $\alpha$  phase [59]. The structure is transformed into a 'body-centered cubic' (bcc) crystal structure at 883 °C, labeled as the  $\beta$  phase [59–62]. This temperature is called ' $\beta$ -trans', which refers to the temperature transition from  $\alpha$  phase or  $\alpha$ - $\beta$  phase to  $\beta$  phase.  $\beta$ -trans is the lowest temperature at 100%  $\beta$  [59].

Titanium alloys are divided into non-alloyed titanium,  $\alpha$ ,  $\beta$ , and  $\alpha$ - $\beta$  titanium alloys [59,63–65]. Unalloyed titanium can be divided into grades 1, 2, 3, and 4, which can be used as implants. The  $\alpha$  alloy has a complete  $\alpha$  structure. The  $\beta$  titanium alloy can be quenched into cold water on its  $\beta$  cross-section, and the  $\beta$  phase has no decomposition of martensite. At room temperature,  $\alpha$ - $\beta$  alloy is the combination of  $\beta$  phase and  $\alpha$  phase. The alloying elements in titanium alloy are divided into  $\alpha$  stabilizer and  $\beta$  stabilizer [66,67]. Alpha stabilizers, such as aluminum and oxygen, can increase the temperature at which the alpha phase is stable.  $\beta$  stabilizers, such as vanadium and molybdenum, are responsible for the constancy of the  $\beta$  phase at lower temperatures [68,69]. Table 1 shows some common types of titanium alloys and their mechanical energy, including elastic modulus, yield strength, and tensile strength.

**Table 1.** Mechanical properties of titanium and some of its alloys.

Alloy Designation	Microstructure	Elastic Modulus <i>E</i> (GPa)	Yield Strength YS (MPa)	Ultimate Strength UTS (MPa)
CpTi	$\alpha$	105	485	580
Ti-3Al-2.5V	$\alpha$	118	550	620
Ti-2.5Al-2Zr-1Fe	$\alpha$	110	570	900
Ti-4Al-2V	$\alpha$	107	860	960
Ti-4Al-0.005B	$\alpha$	107	636	710
Ti-10V-2Fe-3Al	metastable $\beta$	104	1063	1150
Ti-15V-3Cr-3Sn-3Al	metastable $\beta$	80	742	785
Ti-15Mo-3Nb-0.3O	metastable $\beta$	82	1020	1020
Ti-35Nb-5Ta-7Zr	metastable $\beta$	55	530	590
Ti-35Nb-5Ta-7Zr-0.4O	metastable $\beta$	66	976	1010
Ti-6Al-4V	$\alpha + \beta$	110	900	970
Ti-6Al-7Nb	$\alpha + \beta$	105	921	1024
Ti-6.5V-3.5Mo-1.5Zr-0.3Si	$\alpha + \beta$	110	900	1030
Ti-5Al-2.5Fe	$\alpha + \beta$	110	921	1024
Ti-13Nb-13Zr	$\alpha + \beta$	79	900	1030

## 3. Tribocorrosion Behavior

Tribocorrosion behavior usually refers to the damage phenomenon that occurs under the action of friction motion and a corrosive medium [70–72]. Compared with wear damage, the movement of the contact surface in the process of tribocorrosion not only directly wears the material but also destroys the protective film so that the surface of the fresh material continuously contacts the corrosive fluid to accelerate the corrosion, forming

an interaction between corrosion and wear [73–75]. Therefore, coupled tribocorrosion damage is a superposition of tribocorrosion damage and a significant increase in material loss due to corrosion, wear, and their interaction [76–80].

Tribocorrosion is produced under the combined action of corrosion and wear, so many severe influencing factors exist. The main elements are the medium, material, working conditions, and electrochemical characteristics (Figure 2). The typical factors are [81–85]:

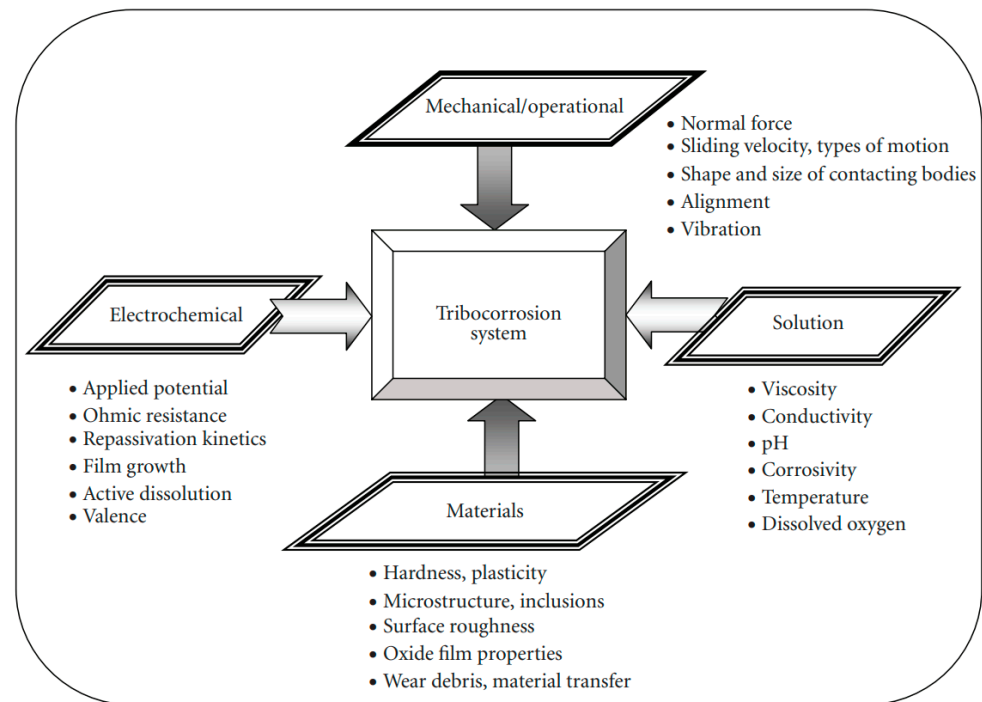


**Figure 2.** Factors influencing tribocorrosion. Adapted from Ref. [86].

- Corrosive medium

The factors that affect the corrosion performance of the material, such as the pH value, medium concentration, and temperature, also influence the tribocorrosion performance of the material. On the one hand, the corrosive medium directly produces corrosion. On the other hand, the medium can react to form new corrosive substances and increase the corrosion wear of the material.

- Wear condition

Similar to traditional tribology, the tribocorrosion properties of materials are closely related to the contact mode (such as point, line, or surface contact), motion mode (such as rolling, sliding, or vibration), load, speed (frequency), and other factors between friction pairs. The results show that the speed and load have the most significant influence on the tribocorrosion properties of the passivation metal, which not only affects the structure and properties of the friction contact surface of the passivation metal but also affects the formation and destruction of the passivation film.

- Material chemical composition and microstructure properties

The main factors affecting the tribocorrosion resistance of materials are the chemical composition, microstructure, hardness, plasticity, and surface roughness. Therefore, wear-resistant and corrosion-resistant integrated materials need to have excellent tribocorrosion resistance, which needs to be comprehensively optimized from chemical composition and microstructure aspects. The structure and mechanical properties of the material are the decisive factors determining its tribocorrosion properties. Only when the material has good tribocorrosion resistance can it be applied to a corrosive wear environment.

- Electrochemical factors

Electrochemical factors include the applied potential, formation, and destruction of passivation film, etc., which are also external factors affecting the tribocorrosion of materials.

To quantify the effect of tribocorrosion on the whole tribocorrosion process, Annsley Mace et al. [87] measured each influencing factor ( $V_T$ ,  $V_P$ ,  $V_I$ , and  $V_{ICPMS}$ ) using various techniques. Figure 3 shows a schematic of the overall process of tribocorrosion. They believe that the total volume of the material ‘removed’ is a groove ( $V_{tr}$ ) caused by the cyclic sliding of a single diamond in the metal, including the generation of plastically deformed metals and wear particle fragments (metals and oxides) on the surface and below. Secondly, there are accumulated materials around the groove. Ideally, since plastic deformation is an equal-volume process, the amount of track ( $V_P$ ) produced by plastic deformation should be similar to the volume of accumulated plastic deformation materials. The  $V_{ICPMS}$  was obtained by measuring the metal ions and fine suspended particles in the solution using ICP-MS. Finally, the instantaneous measurement of the fretting corrosion current during the fretting process provides a method to determine the charge associated with the passivation reaction (i.e., oxide formation) and any anodic ion dissolution reaction and is related to the current-based volume ( $V_I$ ). The volume balance analysis compares the importance of the groove with other volume definitions. Ideally, the two volumes will be equal, according to:

$$V_{tr} = V_{pl} + V_m + 1/PB \cdot V_{ox} + V_{ion} \quad (1)$$

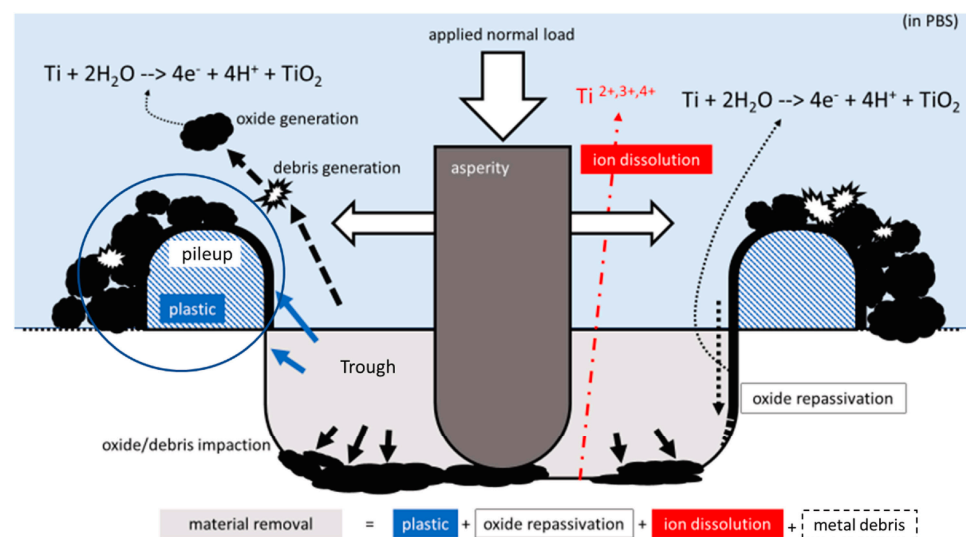


**Figure 3.** Schematic of the proposed process of tribocorrosion (measured by the volume of material removed) with a single asperity, composed of a combination of tribocorrosion mechanisms (plastic deformation, oxide passivation, and ion dissolution) [87].

The amount that can be measured in the experiment has the following relationship:

$$V_P = V_{pl} + V_m + V_{ox} \quad (2)$$

Among them,  $V_{TR}$  is the volume of the cell,  $V_{pl}$  is the volume based on plastic deformation in the accumulation,  $V_m$  is the volume of the metal particles related to the volume of the collection,  $V_{ox}$  is the volume of the generated oxide fragments, and  $V_{ion}$  is the volume of the metal released into the solution as an ion. The constant PB is the Bedworth ratio of Ti.

According to two Formulas (1) and (2), and introducing the sum of the tribological volume and the corrosion volume ( $V_{TC}$ ), consider the volume of ions released into the solution  $V_{ICPMS}$ ; the following relationship is finally obtained to characterize the total friction corrosion volume loss:

$$V_{Tc} + V_c + V_{wear} = V_p + V_I (1 - PB) + V_{ICPMS} \cdot PB \quad (3)$$

Assuming that the measured charge directly produces metal oxides (mainly  $TiO_2$ ),  $V_I$  can be measured using constant potential measurement and estimated according to Faraday's law.

The steps and equipment of tribocorrosion characterization can refer to the research of Mathew et al. [88]. They first performed basic electrochemical tests using a standard three-electrode setup (Figure 4a). A saturated calomel electrode (SCE) was used as the reference electrode, a graphite rod was used as the auxiliary electrode, and the exposed surface of Ti was used as the working electrode. The potentiometer was connected to the computer for data acquisition for corrosion measurement. The open circuit potential (OCP) was initially monitored within 3600 s to assess the potential and stabilize the system. In addition, the sample was circularly polarized from  $-0.8$  V to  $1.8$  V at a scan rate of  $2$  mV/s. The friction corrosion test equipment is shown in Figure 4b. The tribological system consists of an alumina ceramic ball rubbed against a Ti sample (pin with a flat surface) in an electrolyte chamber. The standard three-electrode model shown in the basic electrochemical test was used. The friction corrosion test adopted the classic scheme (Figure 4c). Initially, the sample was electrochemically cleaned at a cathodic potential of  $-0.9$  V<sub>vs. SCE</sub>. This was carried out to achieve the same start-up conditions. The OCP was then monitored within 600 s to evaluate the potential and stabilize the system (using a newly formed  $TiO_2$  film). Next, electrochemical impedance spectroscopy (EIS) tests were performed to study the properties of the oxide film formed on the Ti surface (corrosion kinetics). The frequency range of EIS measurement was 100 kHz to 5 MHz, and the amplitude of the AC sine wave was ten mV, oscillating near the corrosion potential. The potential and current were measured to determine the fundamental ( $Z'$ ) and imaginary ( $Z''$ ) components of the impedance, plotted with a Nyquist plot, or the total impedance ( $|Z|$ ) and phase angle.

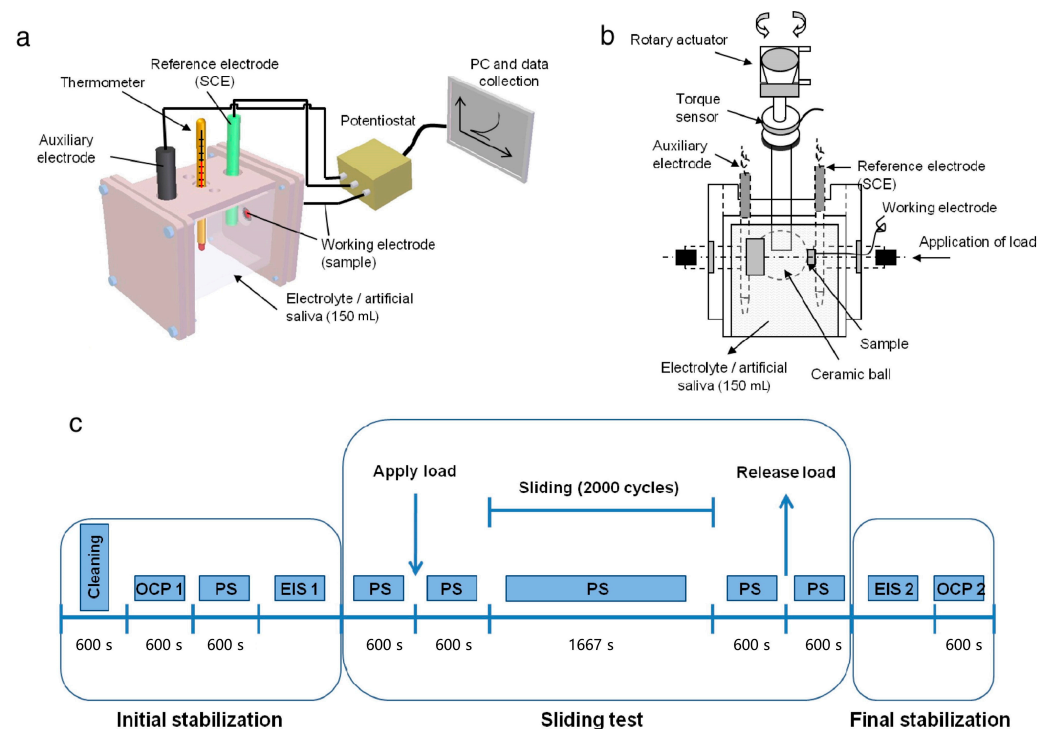


**Figure 4.** (a) Schematic electrochemical setup (a standard 3-electrode cell) used during basic corrosion test. (b) Schematic tribocorrosion setup. (c) Standard protocol used during tribocorrosion test (OCP—open circuit potential; PS—potentiostatic test; EIS—electrochemical impedance spectroscopy) [88].

#### 4. Tribocorrosion Behavior of Titanium Alloy

##### 4.1. Tribocorrosion Behavior of Titanium Alloys in the Marine Environment

There are a variety of inorganic salts dominated by NaCl in seawater, dissolved oxygen, particulate organic matter, and humic substances, including humic acid.  $O_2$  and  $CO_2$  in surface seawater are near saturation, and the pH is about 8.2. It is a corrosive electrolyte solution with a very complex composition. Corrosion-accelerated wear is mainly manifested as  $Cl^-$  leads to brittle spalling of the material surface, increases corrosion activity, destroys the passivation film, and promotes wear [89]. The wear-accelerated corrosion is mainly manifested in the removal of surface corrosion products by friction and wear, the destruction of surface passivation, and  $Cl^-$  hindering the repair of the passivation film. The formation of electrochemical primary cells around the wear scar accelerates the corrosion. Wear also leads to an increase in the specific surface area of the wear surface, resulting in plastic deformation, so that the surface is in a high-energy reactive state and promotes the occurrence of corrosion [90,91].

The synergistic interaction between tribocorrosion in corrosion wear of metals or alloys is usually positively correlated, which promotes each other and accelerates corrosion wear. Zhang et al. [92] compared the fretting wear mechanism and characteristics of TC4 titanium alloy in pure water and a 3.5% NaCl (mass fraction) solution. They found that the process of corrosion, wear, corrosion, and wear showed a 'positive interaction' relationship; that is, the interaction between corrosion and wear aggravated the loss of materials. Chen et al. [93] found that the wear amount of Ti6Al4V in seawater was significantly greater than that in pure water when paired with  $Al_2O_3$  in purified water and simulated seawater, indicating that corrosion accelerated wear.

Pejaković et al. [45] studied the tribo-electrochemical properties of Ti6Al4V under three contact loads (10 mN, 100 mN, and 1 N) in artificial seawater. The results suggest a wear mechanism, as shown in Figure 5. At the lowest load (10 mN), the tangential force in the sliding direction is not strong enough to remove the passivation film, resulting in sliding occurring at the top of the asperities without wearing the film, leading to a lack of wear. Under the highest load, the tangential force is large enough to cause the passivation layer to break and cause significant wear, exposing the metal to a corrosive environment. This is a common situation reported in friction corrosion experiments using point contact. The contact pressure increases sharply under the typical normal load in the Newton range. Under an intermediate load of 100 mN, the average load is assumed to reach a critical value, resulting in the removal of the convex part, which leads to the partial passivation of the metal observed in the friction corrosion experiment and the presence of oxide fragments in the wear traces.

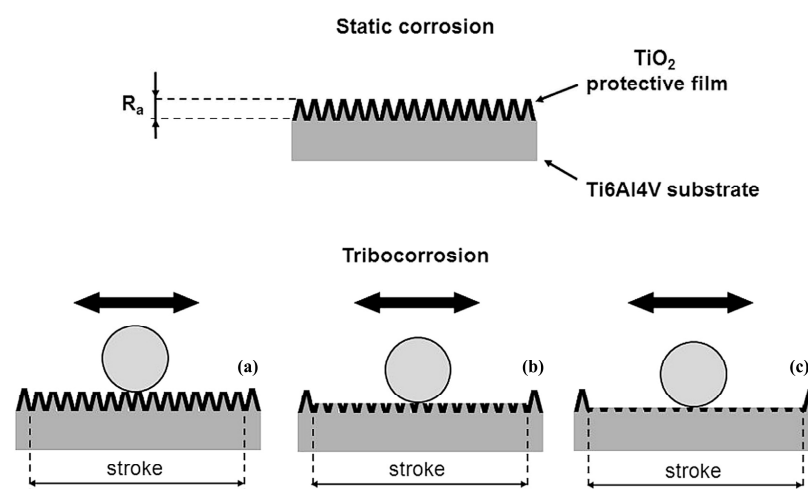
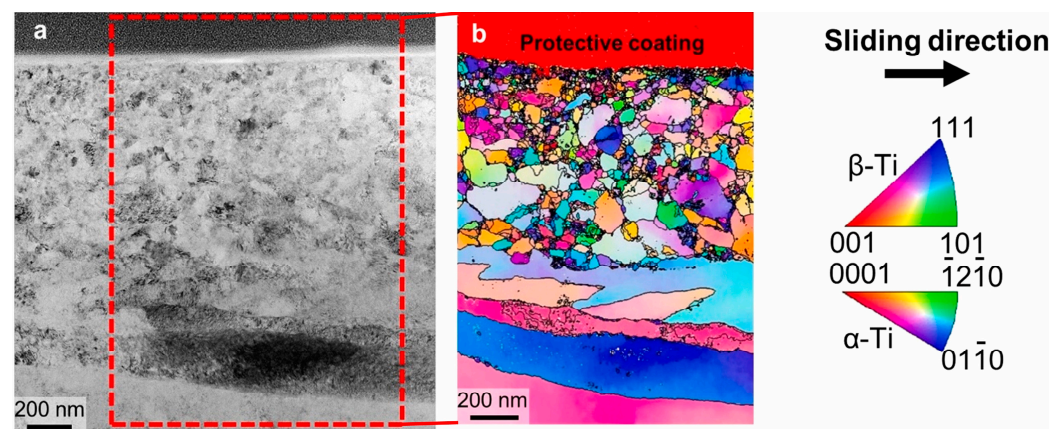


Figure 5. Wear-accelerated corrosion mechanism: (a) 10 mN; (b) 100 mN; (c) 1 N [45].

Ding et al. [94] studied the fretting wear characteristics of TC11 titanium alloy in pure water and simulated seawater. The material loss in seawater is always less than that in water, and the tribocorrosion is a negative interaction. The analysis shows that under fretting conditions, the film produced by active components such as sulfur, phosphorus, and chlorine in seawater plays a role in reducing friction and controlling wear, preventing the generation of a large number of abrasive particles, reducing or even eliminating the damage caused by ‘micro-cutting’ and ‘plowing’ so that corrosion shows a negative interaction in wear.

Xv et al. [95] studied a novel approach  $\beta$  and  $\alpha + \beta$  Friction corrosion behavior of bi-medical titanium alloy in bovine serum solution under open circuit potential. At slower sliding speeds, the alloy has the ability to re passivate. The results show that re passivation is mainly related to the formation of a larger friction film on the worn surface. The friction layer, as a solid lubricating film, stabilizes the friction coefficient. Figure 6 shows the layered structure on the surface of the sample.



**Figure 6.** STEM images of an FIB section of the worn surface of the Ti64ELI. (a) Bright-field image, (b) crystal orientation image using precession electron diffraction [95].

There is no simple tribocorrosion between metal motion pairs in the marine environment. Scholars usually divide the interaction with tribocorrosion into two categories: positive and negative interactions with tribocorrosion. The positive interactions can be divided into the promoting effect of corrosion on wear and the promoting effect of wear on corrosion. Similarly, the negative interactions can be divided into the inhibition of corrosion on wear and the inhibition of wear on corrosion. Moreover, positive and negative interactions are not immutable; they will interact, transit, and transfer under different materials, working conditions, and environmental conditions.

#### 4.2. Tribocorrosion Behavior of Titanium Alloys in the Human Body Environment

Titanium alloy has been used in joint replacement, bone fixation, dental implants, cardiac pacemakers, artificial heart valves, stents, and high-speed blood centrifuges [27,96–100]. However, the elastic modulus of the medical titanium alloys currently used is as high as 90–115 GPa, which is much higher than that of human cortical hard bone (10–25 GPa) and cancellous bone or cartilage (0.05–3 GPa) [101–105]. Such a significant difference in elastic modulus will lead to an unbalanced stress distribution between the implant and the surrounding bone tissue, resulting in stress shielding and loosening of the implant relative to the bone tissue [105–112].

Porous titanium alloy materials have an elastic modulus matching that of human bone tissue, effectively solving the elastic mismatch between implants and human bone [113–119]. Recently, additive manufacturing technology has been used to prepare porous titanium alloy materials [120–125]. This method uses tool software such as 3DXpert (France) and Simulate Additive (Sweden) to design the absorbent structure. Then, the computer controls the laser beam/electron beam layer-by-layer melting process according to the program



and obtains a porous material entirely consistent with the expected structure [126,127]. Three-dimensional printing technology has the advantages of precise digital preparation, high efficiency, a short cycle, and customization [128–130]. It benefits preparing medical metal porous implant devices with complex structures. The large number of pores inside the porous material is more conducive to the growth of surrounding cells and the growth of new bone, thus significantly promoting the ability of bone tissue formation [131–133]. Therefore, porous titanium alloy implant devices have become a research hotspot in metal implants. However, due to the high melting point of titanium alloy and its good affinity with  $O_2$  and  $N_2$  in the air at high temperatures, it is challenging to prepare porous titanium alloy using the liquid foaming method.

Although under normal conditions, the surface of titanium alloy will generate a very stable and continuous oxide passivation film with solid bonding, the passivation film may be peeled off and dissolved under the erosion of external forces and body fluids due to the complexity of the human environment. Therefore, substances will still be released into the tissue during use. In addition, the friction coefficient of titanium alloy is significant and the wear resistance is poor, resulting in a large amount of Ti, Al, and V black debris due to wear after implantation, causing aseptic loosening and eventually leading to joint replacement failure. In addition, Al and V elements have potential cytotoxicity, which may lead to the inability to form apatite on the surface, especially Al, which may cause Alzheimer's disease. Figure 7 shows the characteristic severe corrosion images of the total hip prosthesis components and the recycled Ti6Al4V conical samples [134].

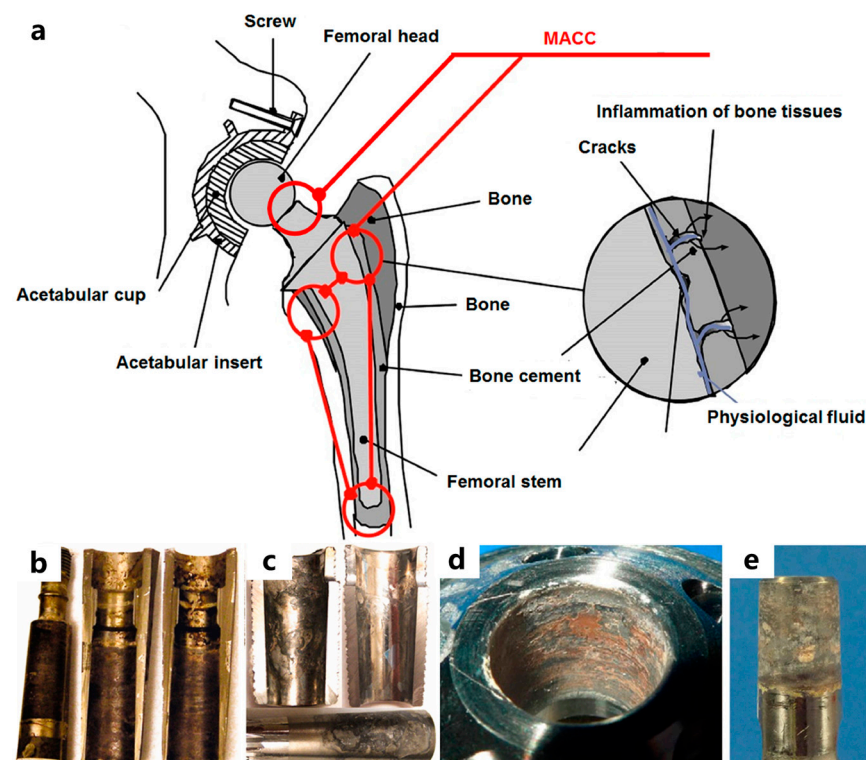


**Figure 7.** (a) Total hip replacement implants [135]; (b) lateral male taper and medial half-sleeve female tapers after 22 months implantation, (c) proximal female and male tapers after 27 months implantation [136], (d) female taper adapter, and (e) male stem taper after 43 months implantation [137].

When titanium alloy is used as a dental implant in a complex oral environment, the implant will be subjected to different forces during the chewing process, resulting in micromotion at multiple interfaces, forming a tribocorrosion system. Vieira et al. [138] studied the effects of varying pH values and corrosion inhibitors on pure titanium during tribocorrosion in artificial saliva. They showed that the tribocorrosion properties are slightly improved after adding citric acid/anode corrosion inhibitor. The reason may be that the

redox reaction occurs in the contact area during the fretting process, forming a passivation layer in the contact area. The hardness of dental implant materials is significantly higher than Young's modulus of bone. The unevenness of relatively rigid materials will eventually penetrate the surface of relatively soft materials, a phenomenon known as microplowing. In Figure 8, the abrasive particles in each movement form a plow, forming a symmetrical furrow. The subsequent groove is parallel to the direction of the abrasive in motion. The proximity of this phenomenon is not conducive to relatively soft materials, causing substantial local deformation and material removal [139].

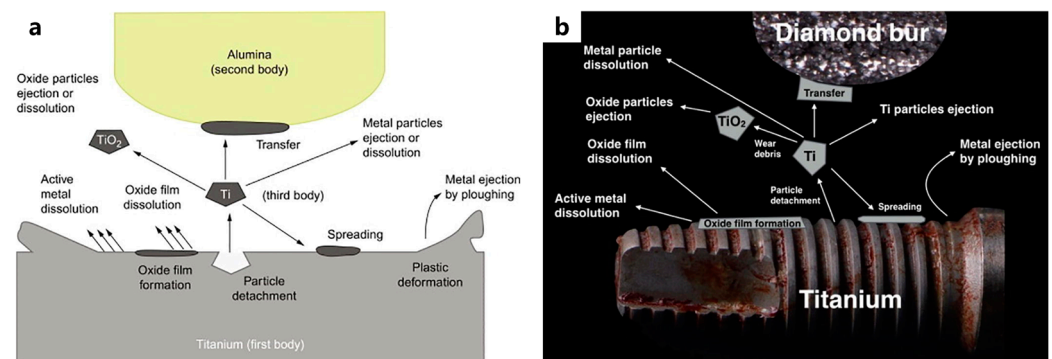


**Figure 8.** (a) Three-body abrasions at the surface of the implant material [140], (b) degradation of a titanium implant due to microplowing and active metal dissolution phenomena [141].

## 5. Surface Modification Methods

Surface strengthening treatment is an effective technical means to improve the tribo-corrosion resistance of titanium alloy. Many surface treatment technologies are applicable for enhancing the feeling of titanium alloy [27,142–144]. The application and development of titanium surface treatment technology have gone through three stages: The first stage is the traditional surface technology represented by electroplating, electroless plating, and thermal diffusion (nitriding, carburizing, etc.). The second stage is the modern surface treatment technology marked by plasma and electron-beam coating technology, laser surface strengthening, thermal spraying, and micro-arc oxidation technology. The third stage is the composite application of various surface treatment technologies. The multi-element, multilayer, gradient structure, and ultra-thick design and preparation of the surface modification layer meet the surface protection requirements of titanium metals in high-speed, heavy-load, and harsh complex-media environments [80,145,146].

Compared with the development of new materials, surface modification has significant advantages and operability in terms of cost. The modification technology of medical titanium alloy is mainly divided into dry amendment and wet modification [1,146]. Dry modification technology carries out various chemical reactions or thin-film deposition on the surface of the titanium alloy substrate in the gas phase, such as magnetron sputtering, vapor deposition, ion implantation, laser cladding, ion beam sputtering, and so on. Wet modification technology is mainly a chemical reaction between the titanium alloy matrix and the elements in the solution environment to achieve surface modification, such as electrochemical deposition, hydrothermal synthesis, and other methods. Table 2 summarizes some surface modification methods and their effects on tribocorrosion properties:

**Table 2.** Common surface modification methods for improving the tribocorrosion resistance of titanium alloys.

	Materials (Protective Layer)	Surface Treatment	Protective Layer Thickness [ $\mu\text{m}$ ]	Environment	Counterpart	Load [N]	OCP Values (V)	$E_{\text{corr}}$ (V)	$I_{\text{corr}}$ ( $\text{A}/\text{cm}^2$ )	Friction Coefficient	Wear Coefficient [ $\text{mm}^3/\text{Nm}$ ]	Main Wear Mechanism
Fei Zhou [147]	Ti6Al4V			aerated artificial seawater	SiC Ball [8 mm]	3 N	−0.8	−0.53	$1.86 \times 10^{-5}$	0.23		
	CrMoSiCN coatings	closed-field unbalanced magnetron sputtering	~1				−0.34	−0.30	$2.22 \times 10^{-7}$	0.12		three-body abrasion mechanism
Andre Hatem [148]	Ti6Al4V			phosphate-buffered saline (PBS) solution	$\text{Al}_2\text{O}_3$ Ball [6 mm]	10 N	−0.95		$7.4 \times 10^{-6}$	0.4	$2.61 \times 10^{-4}$	fatigue wear mechanism
	TiSiCN coatings	plasma-enhanced magnetron sputtering	8–10				−0.3		$6.8 \times 10^{-7}$	0.27	$7.56 \times 10^{-7}$	silicon amorphous restrains the combined action of tri-bicorrosion
Lucia Mendizabal [149]	cp-Ti			PBS solution	$\text{Al}_2\text{O}_3$ Ball [10 mm]	3 N	−1.07			0.58	$4.9 \times 10^{-8}$	
	TaN	magnetron sputtering	2.5				−0.96			0.25	$2.4 \times 10^{-9}$	
Jacek Grabarczyk [150]	Ti6Al4V			PBS solution	$\text{Al}_2\text{O}_3$ Ball	10 N	−0.7			0.35	$1.18 \times 10^{-3}$	mechanism of adhesive wear
	DLC	magnetron sputtering	1~1.5				−0.1			0.08	$4.8 \times 10^{-6}$	combination of adhesive and abrasive wear
T.M. Manhabosco [151]	Ti6Al4V			PBS solution	$\text{Al}_2\text{O}_3$ Ball [5 mm]	4 N	−0.8		$6.2 \times 10^{-7}$	0.3		
	TiN, Ti <sub>2</sub> N	chemical heat treatment	~1				−0.4		$5.8 \times 10^{-5}$	0.45		

Table 2. Cont.

	Materials (Protective Layer)	Surface Treatment	Protective Layer Thickness [ $\mu\text{m}$ ]	Environment	Counterpart	Load [N]	OCP Values (V)	$E_{\text{corr}}$ (V)	$I_{\text{corr}}$ ( $\text{A}/\text{cm}^2$ )	Friction Coefficient	Wear Coefficient [ $\text{mm}^3/\text{Nm}$ ]	Main Wear Mechanism
B. Rahmatian [152]	Ti6Al4V			PBS solution	$\text{Al}_2\text{O}_3$ Ball [5 mm]	15 N	−0.75	−0.28		0.33	$3 \times 10^{-4}$	
	TiB <sub>2</sub> , TiB	chemical heat treatment	~7				−0.6	−0.1		0.37	$1 \times 10^{-5}$	
Kai yuan Cheng [153]	Ti6Al4V			bovine-calf serum	$\text{Al}_2\text{O}_3$ Ball [14 mm]	16 N	−1	0.556	$3.8 \times 10^{-8}$	0.45		mechanism of adhesive wear
	TiC, TiO	chemical heat treatment					−0.15	0.466	$7.18 \times 10^{-7}$	0.18		lubrication mechanism
K.M. Li [154]	Ti6Al4V			HF + HNO <sub>3</sub> corrosion solution	$\text{Al}_2\text{O}_3$ Ball [9 mm]	5 N	−1	−0.86	$1.1 \times 10^{-5}$	0.5		
	TiN	chemical heat treatment	65				−0.6		$4.3 \times 10^{-6}$	0.25		
I. Çaha [155]	cp-Ti			0.9 wt.% NaCl	$\text{Al}_2\text{O}_3$ Ball [10 mm]	1 N	−0.4	−0.371	$1.37 \times 10^{-6}$	0.4	$5.2 \times 10^{-7}$	combination of abrasive and adhesive wear
	TiN	chemical heat treatment	0.3				−0.3	0.009	$7 \times 10^{-8}$	0.6	$7.4 \times 10^{-8}$	abrasive and adhesive wear, fatigue wear
R. Bayón [156]	Ti6Al4V			PBS solution	$\text{Al}_2\text{O}_3$ Ball [10 mm]	5 N	−0.9			0.47	0.74	corrosion–abrasion combination
	DLC	arc ion plating	3.03~3.86				−0.06			0.18	$4.4 \times 10^{-4}$	

Table 2. Cont.

	Materials (Protective Layer)	Surface Treatment	Protective Layer Thickness [ $\mu\text{m}$ ]	Environment	Counterpart	Load [N]	OCP Values (V)	$E_{\text{corr}}$ (V)	$I_{\text{corr}}$ ( $\text{A}/\text{cm}^2$ )	Friction Coefficient	Wear Coefficient [ $\text{mm}^3/\text{Nm}$ ]	Main Wear Mechanism
Yue Wang [157]	Ti6Al4V			artificial seawater	ZrO <sub>2</sub> [6 mm]	5 N		−0.27	$4.03 \times 10^{-7}$		$3.2 \times 10^{-7}$	
	TiSiCN	arc ion plating	2.21~2.47				−0.225	−1.95	$3.65 \times 10^{-7}$	0.15	$3.08 \times 10^{-7}$	sliding friction transforming to rolling friction
Yebiao Zhu [158]	Ti6Al4V			artificial seawater	SiC [6 mm]	5 N		−0.66	$9.4 \times 10^{-6}$		$2.46 \times 10^{-4}$	
	TiSiN/Ag	arc ion plating	2					−0.33	$1.2 \times 10^{-6}$		$4 \times 10^{-6}$	
Minpeng Dong [159]	Ti6Al4V			artificial seawater	SiC [6 mm]	5 N						
	TiSiCN/Ag	arc ion plating	1.905~2.196				−0.04	−0.19	$1.47 \times 10^{-6}$			
M. Faze [160]	Ti6Al4V			0.9 wt.% NaCl	SiC [7 mm]	5 N	−0.8	−0.265	$3.16 \times 10^{-8}$		$6.67 \times 10^{-8}$	
	TiO <sub>2</sub>	PEO					0.3	0.315	$1.38 \times 10^{-8}$		$2.16 \times 10^{-8}$	
V. Sáenz de Viteri [161]	Ti6Al4V			PBS solution	Al <sub>2</sub> O <sub>3</sub> Ball [10 mm]	3 N	−0.357	0.472				abrasive wear
	Ca,I,P-TiO <sub>2</sub>	PEO	3.1~4.89				−0.001	0.744				adhesive wear
You Zuo [162]	Ti6Al4V			3.5 wt.% NaCl	Al <sub>2</sub> O <sub>3</sub> Ball [6 mm]	2 N	−0.1	−0.25	$6.27 \times 10^{-9}$	0.3		
	graphene oxide-TiO <sub>2</sub>	PEO	6.1				0.4	0.35	$2.28 \times 10^{-8}$	0.35		
Hongwei Zhang [163]	Ti6Al4V			3.5 wt.% NaCl	Si <sub>3</sub> N <sub>4</sub> [6.35 mm]	5 N	−0.72	−0.9	$6 \times 10^{-5}$	0.4		
	TiN + TiB	laser cladding technology					−0.2	−0.6	$2.6 \times 10^{-5}$	0.55		

### 5.1. Chemical Heat Treatment

Chemical heat treatment is a process in which the material is placed in a medium containing a particular active element for heating and heat preservation, and a concentration gradient is formed on the surface to make the active ingredient enter the surface of the material to form a layer [164–167]. Chemical heat treatment can effectively improve the thermal fatigue resistance, wear resistance, and corrosion resistance of materials, and chemical heat treatment has a low cost, wide application, and mature technology [168–175]. After chemical heat treatment, the surface composition of the material will change [176,177]. After chemical heat treatment, the material surface's hardness, strength, wear, and corrosion resistance are greatly improved [178–182].

The chemical surface heat treatment methods mainly include nitriding, carburizing, oxidating, and boronizing. Nitriding treatment is the most commonly used chemical heat treatment method for titanium metal surfaces, including gas nitriding, plasma nitriding, and laser nitriding [183–192]. The nitriding temperature of titanium metal is much higher than that of steel materials. It must be above 800 °C to obtain a nitride layer with sufficient depth. The nitrogen element infiltrated into the surface of titanium metal forms a nitrogen and titanium solid solution of  $\alpha$  phase and  $\alpha + \beta$  phase, and a thin titanium nitride layer is formed on the outermost layer. The thickness of the hardened layer obtained with a nitriding treatment is generally not more than 200  $\mu\text{m}$ , and the hardness of the nitrided layer is about 10 GPa.

Zhao et al. [193] indicated that plasma nitriding on pure Ti produces a thick, dense, and homogeneous TiN layer similar to DLC coating. This provides a comparatively better performance as an implant biomaterial, since it exhibited excellent electrochemical, tribological, and tribocorrosion performance. Wang et al. [180] studied the effect of plasma nitriding and TiN coating dual-phase treatment on the corrosion resistance of cast titanium. Compared with the untreated titanium, the dual-phase-treated titanium showed a higher corrosion potential ( $E_{\text{corr}}$ ) and lower corrosion current density ( $I_{\text{corr}}$ ). The SEM results showed that the surface corrosion of untreated titanium was more severe than that of dual-phase-treated titanium. Guan et al. [194] used a self-made induction nitriding device to nitride medical pure titanium (TA1) and used Hank's solution to test its wear resistance and corrosion behavior. The tribocorrosion behavior and synergistic effect were studied with electrochemical measurements and surface morphology analysis. The experimental results in Figure 9 showed that a nitrided layer of about 20  $\mu\text{m}$  thick could be obtained after one hour of induction nitriding treatment of TA1, which effectively improved the mechanical properties, corrosion resistance, and wear resistance of TA1. The pure wear weight loss and pure corrosion weight loss of nitrided samples were one order of magnitude lower than those of untreated samples. The synergistic effect was produced in friction corrosion, and weight loss caused by wear was dominant. However, the temperature of the chemical surface heat treatment was high, and the treatment time was extended. The high temperature and long-duration chemical heat treatment can easily affect the fatigue performance of titanium metal, and the corrosion resistance was reduced.

Thermal oxidation refers to exposing the material to an oxygen atmosphere in a high-temperature environment to cause an oxidation reaction on the surface [195–197]. Thermal oxidation is usually used to improve the material surface's heat resistance, corrosion resistance, and oxidation stability. By reacting with oxygen at high temperatures, an oxide layer is formed on the material's character, which can increase its surface hardness and reduce the surface friction coefficient. In thermal oxidation, metal materials react with oxygen to produce metal oxides. These oxides form a dense, uniform oxide layer that can adhere to the metal surface. The thickness, composition, and properties of the [198] oxide layer depend on the temperature, oxygen concentration, and thermal oxidation time [75]. The oxide layer has good heat resistance and oxidation stability, which can protect the metal surface from high-temperature oxidation. Secondly, the oxide layer can improve metal materials' corrosion resistance, reduce metals' reaction with external gas and liquid, and prolong their service life.

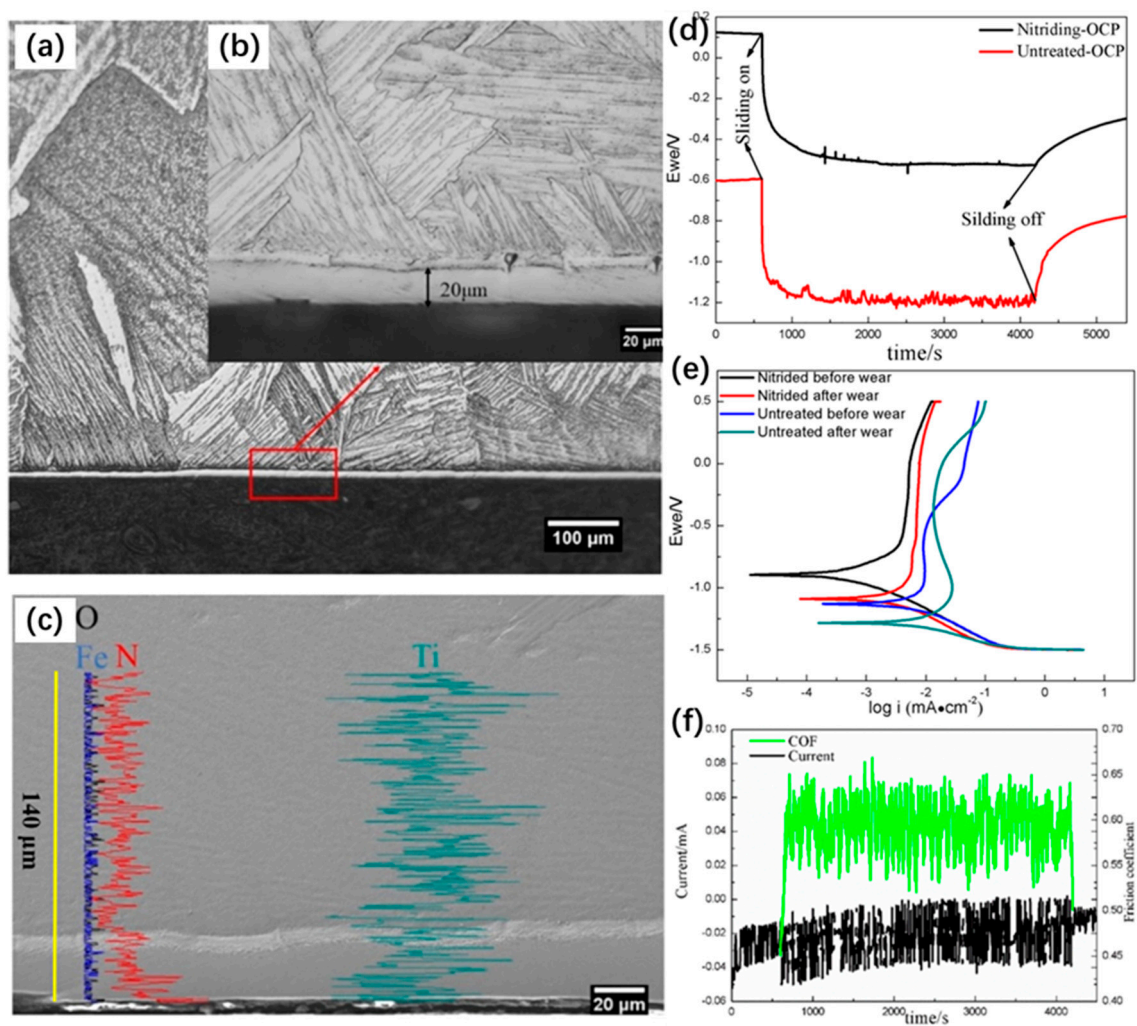


**Figure 9.** (a,b) Cross-section metallography of nitriding sample, (c) cross-section SEM-EDS of nitriding sample, (d) OCP curves of nitriding and untreated sample, (e) polarization curve before and after tribocorrosion, (f) current and COF of nitrided and untreated sample [194].

R. Bailey et al. [199] studied the corrosion and tribocorrosion properties of thermally oxidized commercially pure titanium in a 0.9% NaCl solution. This treatment produces a multilayer structure consisting of a 1 μm rutile (TiO<sub>2</sub>) film and a 9 μm α titanium oxygen diffusion zone (ODZ) (α-Ti(O)). Compared with the untreated CP-Ti, the rutile oxide layer has low friction and better resistance to material removal during tribocorrosion. Four friction zones can be identified in the typical friction curve during the sliding wear under open circuit potential. Each friction zone has characteristics corresponding to the gradual or partial removal of the oxide layer, oxide layer, diffusion zone, and matrix. The abnormal anodic protection behavior of the oxide film is also observed. When titanium is positively polarized during sliding, the durability of the oxide layer is extended, thereby reducing friction and significantly reducing material loss. Cheraghali et al. [200] generated a more biologically active porous anodic oxide layer on the thermal oxide layer with ODL anodic oxidation technology. The effects of the average load and sliding distance on the tribocorrosion behavior of the anodic oxide layer produced using the ODL anodic oxidation process were studied. The results showed that the anodic oxide layer had sufficient durability at sliding distances of 5 m and 25 m and could resist friction stress. However, a further increase in the sliding distance leads to local damage to the oxide layer, which is then completely removed at a sliding distance of 300 m, especially under high

normal loads of 1 and 1.5 N. ODL showed the lowest tribocorrosion rate, followed by anodic oxidation at 150 V and 175 V.

Si et al. [201] prepared a  $\text{TiO}_2/\text{SrTiO}_3$  heterostructure coating on the surface of the Ti6Al4V alloy using thermal oxidation. The preparation process and mechanism of  $\text{TiO}_2/\text{SrTiO}_3$  coating are shown in Figure 10. The effective removal of bacterial biofilm could be achieved under ultraviolet light irradiation. In addition, the tribocorrosion properties of  $\text{TiO}_2/\text{SrTiO}_3$  coatings in SBF solution were also tested. The results showed that a thermal oxide layer with sufficient thickness provides a reliable tribocorrosion protection barrier. The thermal oxide layer was subjected to a periodic contact load and surface fatigue cracks. The wear scar pit was shallow, and the wear debris peeled off from the matrix as scales, a typical fatigue wear characteristic.

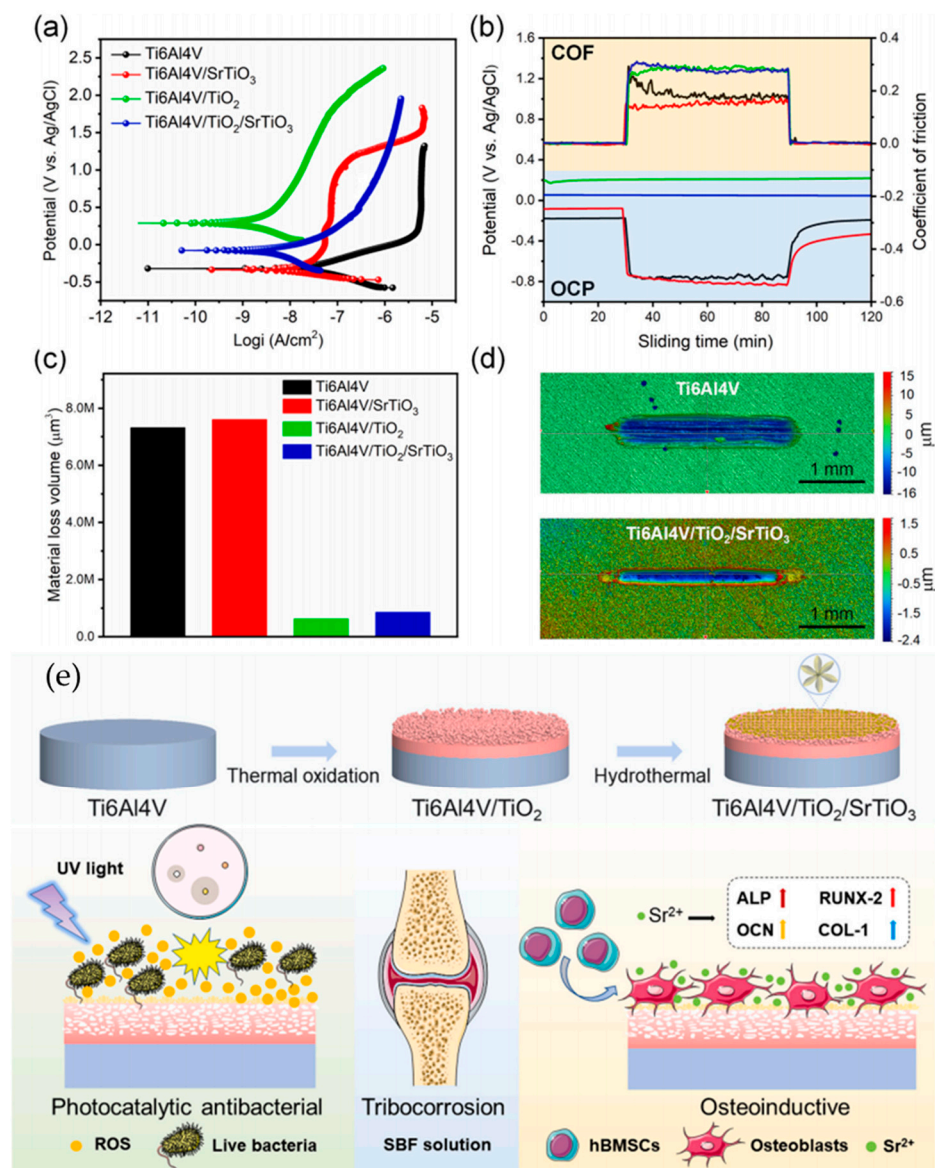


**Figure 10.** Tribocorrosion characterization of different samples: (a) potentiodynamic polarization curves, (b) evolution of OCP and COF with sliding time for Ti6Al4V (black), Ti6Al4V/SrTiO<sub>3</sub> (red), Ti6Al4V/TiO<sub>2</sub> (green) and Ti6Al4V/TiO<sub>2</sub>/SrTiO<sub>3</sub> (blue), (c) material loss volume, and (d) 3D surface morphologies. (e) Schematic diagram of the TiO<sub>2</sub>/SrTiO<sub>3</sub> coating with photocatalytic, antibacterial, osteogenesis, and tribocorrosion resistance properties [201].



## 5.2. Plasma Electrolytic Oxidation

Plasma electrolytic oxidation (PEO), also known as micro-arc oxidation (MAO), is a surface treatment technology [202–205]. Metal materials are placed in the electrolyte, and a micro-arc discharge is generated by applying a high voltage, thus forming an oxide film on the metal surface. This oxide film usually has the characteristics of uniformity, density, and high hardness, which can provide good protection and improve the surface properties of metal materials [206–209]. The PEO process includes electrochemical oxidation, plasma chemical reaction, and thermal diffusion in the electrolyte. Micro-arc oxidation technology can grow a layer of coating in situ with high hardness and wear and corrosion resistance on the surface of valve metals such as titanium, which can significantly improve the surface properties of light metals. In addition, PEO can adjust surface properties such as hardness, elastic modulus, wettability, porosity, roughness, chemical composition, and crystallinity [210–214].

Compared with traditional surface treatment technologies such as anodic oxidation and electroplating, it is an environmentally friendly surface treatment technology with a short process flow and no heavy metal ions in the solution. In addition, the micro-arc oxidation process is stable and reliable, and the equipment is simple. The reaction is carried out at room temperature, which is easy to operate and master. The ceramic film is in situ grown on the substrate, the bonding is firm, and the ceramic film is dense and uniform.

S.A. Alves et al. [215] produced an anodic oxide film on the surface of cp-Ti with plasma electrolytic oxidation (PEO) technology. After PEO treatment, oxide films with varying surface characteristics, such as surface roughness, morphology, and film thickness, were achieved based on the anodic oxidation parameters. To examine the impact of PEO treatment on the tribocorrosion behavior, untreated and PEO-treated Ti samples were subjected to a reciprocating sliding test in artificial saliva. The results showed that PEO treatment effectively enhanced the resistance of the cp-Ti substrate to both electrochemical and mechanical influences, and the efficacy was influenced by the specific PEO process parameters employed. Laurindo et al. [216] evaluated the effect of PEO voltage and annealing treatment on tribocorrosion properties. The results showed that the PEO layer significantly improves the tribocorrosion resistance of bare titanium. A rutile phase also increases friction corrosion resistance through voltage or post-heat treatment. Sukuroglu et al. [217] used different frequencies to grow TiO<sub>2</sub> coatings on Cp-Ti substrates, and the treatment method was PEO. The tribocorrosion properties of the coating were studied with a pin-on-disk wear test and potentiodynamic polarization test device. The effect of frequency change on the performance of the PEO coating was examined at a constant voltage. As a result, the increase in frequency lead to smaller pores and cracks in the surface morphology of the coating, which lead to an increase in the friction and corrosion behavior of the layer.

He et al. [218], in situ, synthesized Cu<sub>x</sub>O (CuO and Cu<sub>2</sub>O) on the ceramic coating on the titanium alloy substrate with plasma electrolytic oxidation (PEO) and systematically studied its biological activity and tribocorrosion behavior. The specific results are shown in Figure 11. During the tribocorrosion process, the formation of hydroxyapatite and CuO on the worn surface prevented direct contact between the coating and the counterpart, resulting in a practical lubrication effect, which reduced the mass loss of the prepared layer by 53.5% compared with the traditional PEO coating. More importantly, the sliding process accelerated the enrichment of Cu on the worn surface, and hydroxyapatite deposition on the dull surface induced the conversion of Cu<sub>2</sub>O to CuO. This behavior produces lubrication and prevents direct contact between the coating and the counterpart. It is worth noting that tribocorrosion is beneficial to long-term antibacterial activity, and a high surface Cu content enhances the long-term antibacterial activity of the Cu<sub>x</sub>O/TiO<sub>2</sub> coating, which provides essential value for the clinical application of long-term sterilization of implant materials.

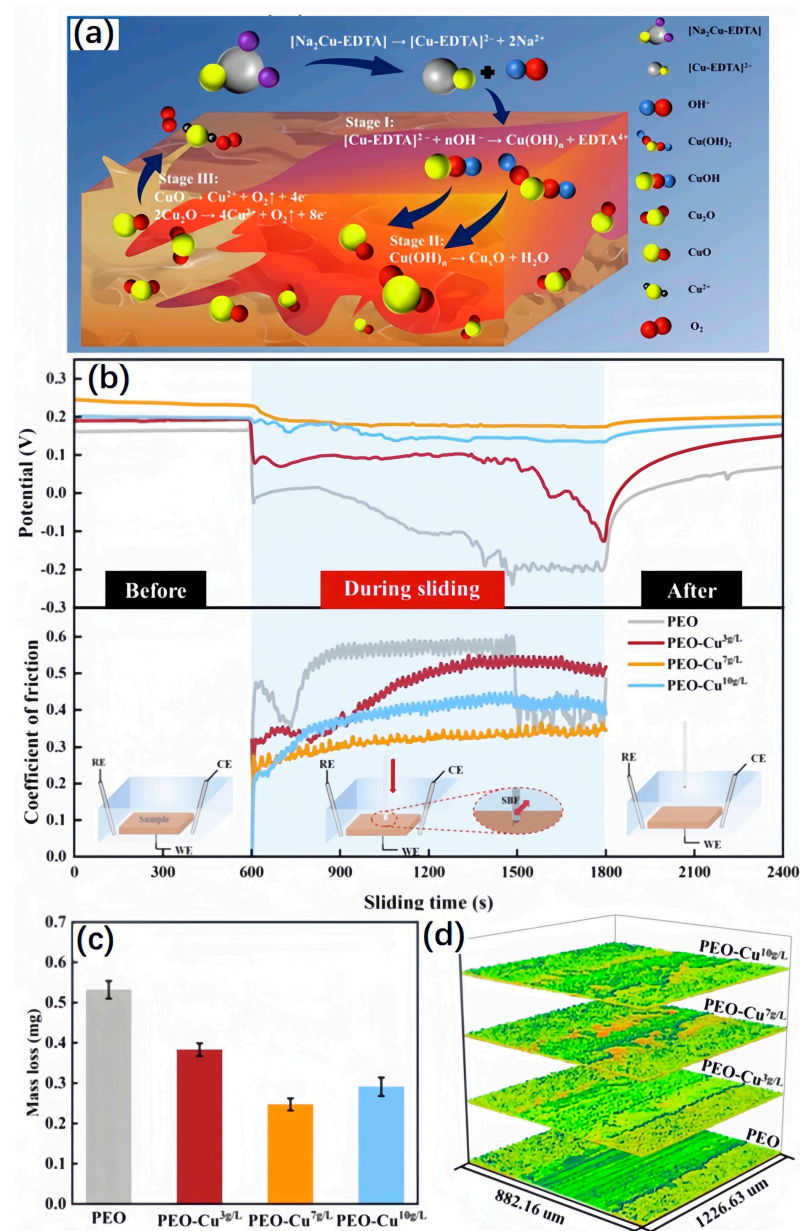


**Figure 11.** (a) Schematic illustration underlying the incorporation mechanism of  $\text{Cu}_x\text{O}$  phases into the  $\text{TiO}_2$  layer, (b) OCP and COF before, during, and after sliding in SBF condition (WE: working electrode, CE: counter electrode, RE: reference electrode), (c) the mass loss, (d) the 3D topographies [218].

The micro-arc oxidation technology was developed based on anodic oxidation [204]. The process has outstanding characteristics: (1) The electrolyte is weakly alkaline and does not pollute the environment. (2) The process is simple. The pretreatment of the workpiece only requires oil removal and decontamination on the surface. It does not need to remove the natural oxide layer on the surface, which is suitable for large-scale automation. (3) Micro-arc oxidation can be completed at once or several times, and anodic oxidation must be restarted once interrupted. (4) No vacuum or low-temperature conditions are required. However, the formation process of micro-arc oxidation films is quite complex, and research on the mechanism is insufficient; the oxidation voltage is much higher than that of conventional anodic oxidation, and safety should be paid attention to during operation. The current efficiency of micro-arc oxidation is low; the electrolyte temperature rises rapidly and needs to be cooled.

### 5.3. Physical Vapor Deposition

Physical vapor deposition (PVD) technology refers to the use of physical methods to vaporize the surface of the material source (solid or liquid) into gaseous atoms or molecules under vacuum conditions or partially ionized into ions, and through a low-pressure gas (or plasma) process, a film with certain special functions is deposited on the surface of the substrate [219–221]. Physical vapor deposition is one of the leading surface treatment technologies. PVD coating technology is divided into three categories: vacuum evaporation, sputtering, and ion coating [222,223]. The main methods of physical vapor deposition are vacuum evaporation, magnetron sputtering coating, arc plasma coating, ion plating, and molecular beam epitaxy. The corresponding vacuum coating equipment includes a vacuum evaporation machine, a vacuum sputtering coating machine, and a vacuum ion coating machine. With advancements in deposition methods and technologies, physical vapor deposition technology has the capability to deposit various types of films including metal films, alloy films, compounds, ceramics, semiconductors, polymer films, etc. By employing various target materials, reaction gases, process methods, and parameters, nitriding enables the production of diverse coatings catering to different needs [224–228]. These coatings include surface-strengthened coatings with exceptional hardness and wear resistance, coatings with high density and chemical stability providing corrosion resistance, solid lubrication coatings, coatings in a wide range of decorative colors, as well as unique functional coatings used in electronics, optics, energy science, and other fields [56,229–232].

Plasma-enhanced magnetron sputtering (PEMS) is a method to improve magnetron sputtering technology using the plasma enhancement effect [233–235]. In the traditional magnetron sputtering process, the surface of the sputtering target is bombarded with ions, resulting in the shedding of the sputtering material. In plasma-enhanced magnetron sputtering, by generating plasma in the sputtering chamber and introducing energetic ions, the ion density and energy can be increased, thereby improving the quality and growth rate of the film [236]. Hatem et al. [148] synthesized a low-friction Ti-Si-C-N nanocomposite coating on ASTM F136 (Ti-6Al-4V ELI) titanium alloy using plasma-enhanced magnetron sputtering (PEMS) technology. The results showed that the wear rate of the low-friction Ti-Si-C-N nanocomposite coating was reduced by at least 97% compared with the bare titanium alloy sample. The tribocorrosion performance of the coating samples strongly correlated with the silicon and carbon content in the chemical composition of the coating. Therefore, the refinement of nanocrystals, the existence of amorphous carbon regions, and the generation of oxides are the related characteristics to improve Ti-Si-C-N nanocomposites' friction and corrosion behavior.

Unbalanced magnetron sputtering is a magnetron sputtering technology that is characterized by the introduction of a non-uniform magnetic field in the magnetron sputtering system to improve the spatial distribution of the electron cloud during the sputtering process, thereby improving the quality and performance of the film [237–240]. Fu et al. [241] prepared CrMoSiN coatings with different molybdenum contents on silicon and titanium alloy substrates with an unbalanced magnetron sputtering system. They tested the tribocorrosion behavior of the coatings sliding with SiC balls in seawater. After the addition of the Mo element to the CrSiN coating, (Cr, Mo) N replaces the solid solution and combines with CrN, Mo<sub>2</sub>N phase, and SiN<sub>x</sub> amorphous to form a nanocomposite structure in the CrMoSiN coating, and the columnar structure is dense. Therefore, the coating surface changes from a 'fine dome' shape to a relatively flat profile with a 'groove boundary'. The columnar structure of the CrSiN coating is loose, and severe coating peeling occurs on its wear track. Under the synergistic effect of tribocorrosion, the material loss of the CrSiN coating begins to accelerate, as shown in the figure. For CrMoSiN coatings, due to the formation of the MoO<sub>3</sub> layer (Figure 12) under polarization and wear behavior, the wear track of all CrMoSiN coatings becomes smooth without coating peeling marks. The three-body wear is eliminated, and the phenomenon of coating peeling is eliminated.

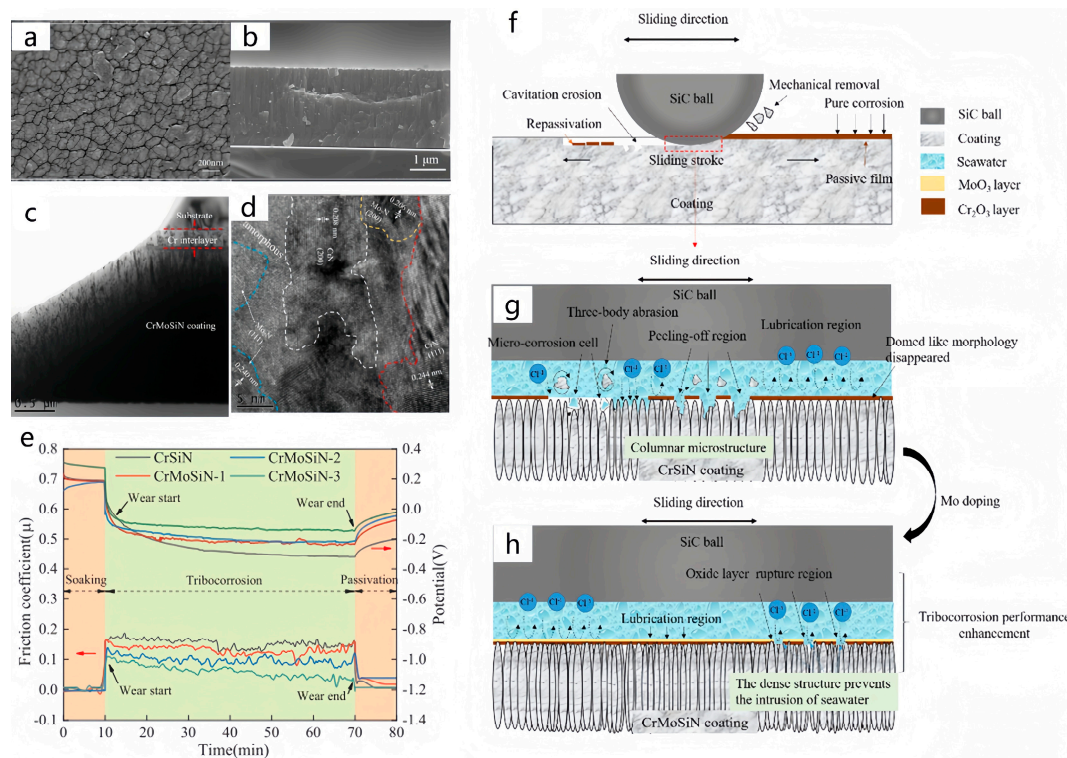


**Figure 12.** Surface and cross-sectional SEM images of CrMoSiN (a,b), TEM (c), and HRTEM (d) images of CrMoSiN coating, (e) OCP measurements and respective friction coefficient curves of CrSiN and CrMoSiN coatings, Schematic illustration of tribocorrosion mechanism for Cr(Mo)SiN coatings in artificial seawater (f–h) [241].

Radio frequency sputtering is a sputtering technology using a radio frequency power supply. It is a physical vapor deposition technology used to form a uniform, dense, high-quality film on the surface of the film material [242–244]. The main working principle of radio frequency sputtering technology is to introduce an inert gas into the sputtering device and make it collide with the atoms or molecules of the sputtering source by accelerating and bombarding the static gas ions. The atoms or molecules of these sputtering sources will be knocked out and form a film on the surface of the substrate material [245,246].

Çaha et al. [155] used sputtering technology to deposit TiN coating on the surface of cp-T to improve its tribocorrosion performance. Figure 13 shows SEM images of the worn scratches and worn sub surfaces, as well as the wear mechanisms of different samples. It was found that the uncoated and 30 min samples were mainly characterized by a combination of abrasive and adhesive wear, which was controlled by parallel grooves, discontinuous friction layers, plastic deformation, and transfer materials. In comparison, the abrasive and sticky wear characteristics of 80 min samples only occurred on the prominent surface. The reason was that with the increase in deposition time, the proportion of the Ti<sub>2</sub>N phase increases, and the corresponding coating exhibits a lower corrosion rate and better capacitance behavior, making it resistant to abrasive wear, adhesive wear, and plastic wear.

Zhao et al. [247] successfully prepared TiN coating and Ti/TiN multilayer coating on the surface of Ti6Al4V alloy using multi-arc ion plating technology. The corresponding characterization and wear mechanism models of different coatings are shown in Figure 14. The Ti/TiN multilayer coating has good friction corrosion resistance and a low friction coefficient. For the TiN coating, the surface compressive stress causes the crack to diffuse below the coating surface, accelerating the coating failure. The soft Ti layer in the Ti/TiN multilayer coating can effectively prevent the generation and propagation of cracks and interrupt the continuous growth of columnar crystals, making the coating more dense and

the corrosive medium not effortless to penetrate the substrate. In the simulated body fluid environment at 37 °C, the tribocorrosion resistance of the multilayer coating is nearly twice as high as that of Ti6Al4V alloy and TiN coating. They concluded that the material loss caused by tribocorrosion is not the sum of superficial, pure corrosion, and pure wear loss, and the synergistic effect between tribocorrosion accounts for a large proportion of the total volume loss. Zhang et al. [248] introduced a metal Zr layer into the ZrN coating to prepare a Zr/ZrN multilayer coating on the surface of titanium alloy, reducing the cylindrical grain boundaries and growth defects of the coating. The Zr layer in the multilayer coating could preferentially form a  $ZrO_2$  passivated film, and the multilayer structure could effectively inhibit the penetration of corrosive media so that it had good corrosion resistance. At the same time, the introduction of Zr metal layer inhibited the crack growth during the wear process and further improved the tribocorrosion resistance of Zr/ZrN multilayer coating. This study revealed the penetration law of corrosive media in the multi-layer coating and the formation mechanism of passivation film on the surface of titanium alloy and clarified the interaction mechanism between corrosive media and cracks in the process of corrosion wear, which can provide a theoretical basis for the further application of multi-layer coating in the surface protection of medical titanium alloy.

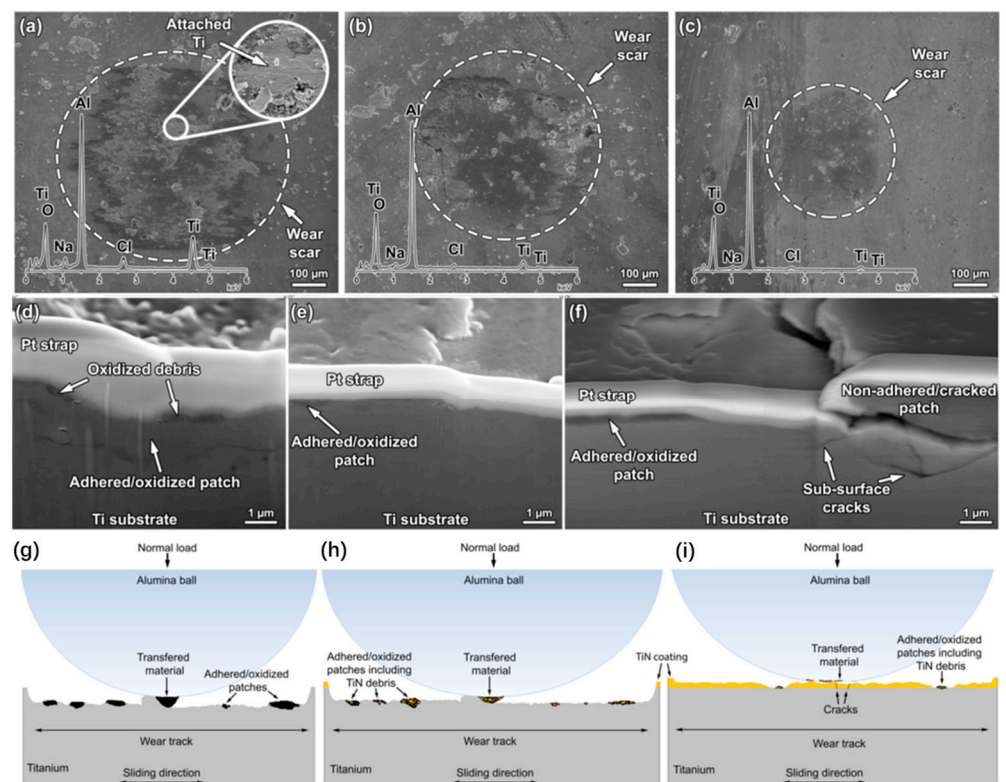


**Figure 13.** (a–c) SEM images of worn scars on the surfaces of different samples, (d–f) magnification SE/SEM images of the worn sub-surfaces of different samples, (g–i) schematic tribocorrosion mechanisms of different samples [155].

Diamond-like carbon (DLC) coatings are known to be excellent candidates for using as protective coatings on biomedical alloys, not only due to their excellent tribological properties but also due to their chemical composition and stability [249–254]. Hinüber et al. [255] fabricated a ta-C DLC on Ti6Al4V alloy, which presented a good adhesion strength, together with reduced tribocorrosion rate in PBS solution and excellent *in vitro* biocompatibility. E. Arslan et al. [256] investigated the tribocorrosion behavior of the Ti6Al4V alloy and the Ti-DLC coating deposited on the Ti6Al4V substrate using closed-field unbalanced magnetron sputtering (CFUBMS) under tribocorrosive conditions in sliding contacts. The open-circuit potentials were affected by rubbing and changed significantly for the Ti6Al4V

substrate and the Ti-DLC coating during rubbing. The tribocorrosion performance of the Ti-DLC coating was better than that of the Ti6Al4V substrate. DLC coatings demonstrated a high protection efficiency (about 97%) against corrosion of the Ti6Al4V substrate, drastically reducing the corrosion current density in static conditions compared to the Ti6Al4V alloy [257]. The tribological properties were significantly improved under dry conditions. However, the life of DLC films was reduced two to ten times in the tribocorrosion tests by the simultaneous action of tribocorrosion mechanisms.

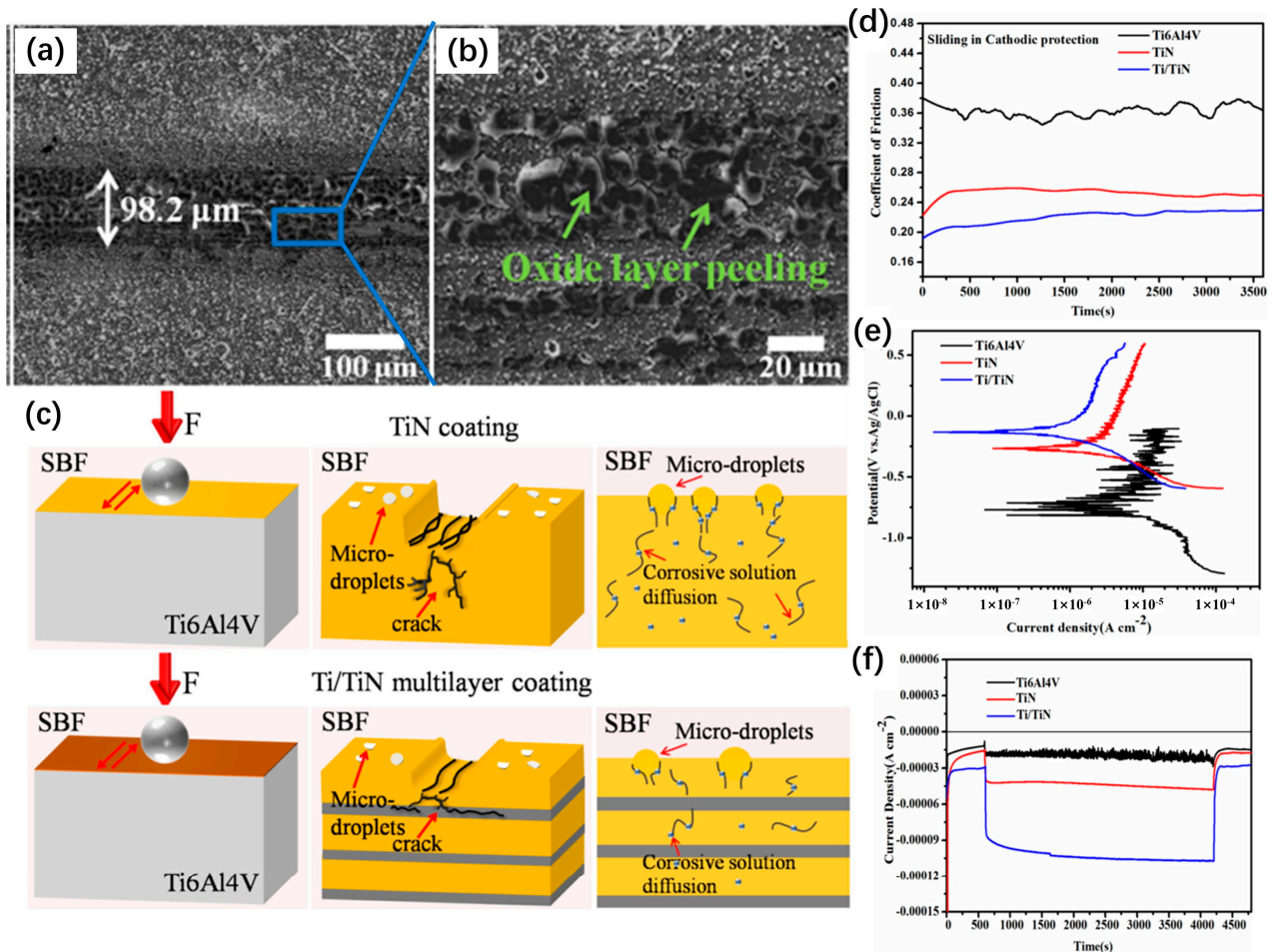


**Figure 14.** (a,b) SEM images of wear track sliding, (c) wear mechanism models of different coatings in simulated body fluid, (d) friction coefficient curves of various coatings, (e) potentiodynamic polarization curves of various coatings, (f) evolution of OCP values of different coatings [247].

At present, hard coatings are usually deposited on the surface of titanium alloy using vapor deposition technology to improve the friction and wear properties of titanium alloy substrates. However, due to the significant differences in hardness, thermal expansion coefficients, and elastic moduli between the hard coating and the titanium substrate, as well as the high residual stress inside the coating, the bonding strength between the coating and the substrate is low, and even brittle cracking and shedding occur. In addition, for single-layer binary and multi-element hard coatings, with the extension of deposition time and the increase in temperature, the grains gradually coarsen and form columnar crystals, resulting in intergranular cracks. Structural defects such as grain boundaries and intergranular microcracks are often fast channels for aggressive ion permeation of coatings.

#### 5.4. Laser Cladding

Laser cladding refers to adding external materials to the molten pool formed with laser irradiation of the substrate, employing synchronous or preset materials and rapid

solidification of the two to create a cladding layer [258–262]. The characteristics of laser cladding include: the cladding layer has low dilution but strong bonding force and is metallurgically bonded to the substrate, which can significantly improve the wear resistance, corrosion resistance, heat resistance, oxidation resistance, and electrical characteristics of the substrate material surface to achieve the purpose of surface modification or repair, meet the specific performance requirements of the material surface, and save a lot of material costs [263–268]. The process parameters of laser cladding mainly include laser power, spot diameter, cladding speed, defocusing amount, powder feeding speed, scanning speed, preheating temperature, etc. These parameters significantly influence the dilution rate, cracking, surface roughness of the cladding layer, and compactness of the cladding parts. The parameters also affect each other, which is a very complex process. It is necessary to adopt reasonable control methods to control these parameters within the allowable range of the laser cladding process.

Feng et al. [37] prepared a new Ti-Al-(C, N) composite coating on TC4 substrate using laser cladding technology. Then, the electrochemical properties of the mixed layer under static and dynamic conditions were analyzed in an artificial seawater environment, and the tribocorrosion behavior and corrosion–wear synergistic mechanism were studied using the tribocorrosion test system. The results show that  $Ti_2AlC$  and  $Ti_2AlN$  self-lubricating phases in the composite coating and the corrosion products with particular lubrication effects produced during the friction process keep the average friction coefficient low. With the increase in load, the mechanical failure of the passive film during the friction process is enhanced, the adsorption of the corrosive medium on the surface of the passive film leads to its active dissolution, and the wear amount increases. The corrosion range of the composite coating in artificial seawater is not extensive, and the wear behavior mainly determines the volume loss caused by friction corrosion.

Obadele et al. [269] used the ytterbium-doped laser system to laser clad commercially pure Ti particles on Ti6Al4V. They also evaluated the tribocorrosion behavior of laser cladding Ti6Al4V on the sliding of alumina balls in 3.5% NaCl. The corrosion potential of the Ti6Al4V-coated sample was lower than that of the uncoated sample. In addition, in the two electrolytes studied, the corrosion current density of the cladding Ti6Al4V was significantly reduced. The tribocorrosion behavior of the cladding Ti6Al4V did not change significantly. The Ti6Al4V cladding layer was greatly reduced in the modified 3.5% NaCl, while it remained unchanged in 3.5% NaCl. In Ti6Al4V, the friction coefficient increased with time, while the friction coefficient of the cladding sample decreased slightly with time. Pejaković et al. [36] developed a 316L laser cladding layer reinforced with titanium carbonitride grains. An agglomerated sintered (Ti, Mo) (C, N) -Ni powder was designed to maintain the chemical integrity of the challenging phase during laser deposition. The tribocorrosion resistance of the sample in artificial seawater was increased by more than ten times under the condition of open circuit potential and by more than thirty times under the condition of passive potential.

Zhang et al. [163] prepared a TiN + TiB/TC4 titanium-based composite coating using laser cladding. The preparation process, characterization of tribocorrosion performance, and wear mechanism are shown in Figure 15. The results showed that adding BN promoted the in situ formation of micro-sized elliptical TiN phases and nano-sized fibrous TiB phases, forming a new structure with the hard TiN surrounded and anchored by coherent TiB. With increasing quantities of TiN and TiB phases, the material did not undergo significant plastic deformation. During the tribocorrosion process, a considerable accumulation of satisfactory debris, repeated compaction, and relative motion on the surface formed a dense  $TiO_2$ - $MoO_3$  oxide film. When exposed to a corrosive chloride ion environment, the thick oxide film transformed into a two-layer structure consisting of a dense inner layer and a porous outer layer, significantly reducing the tribocorrosion rate.

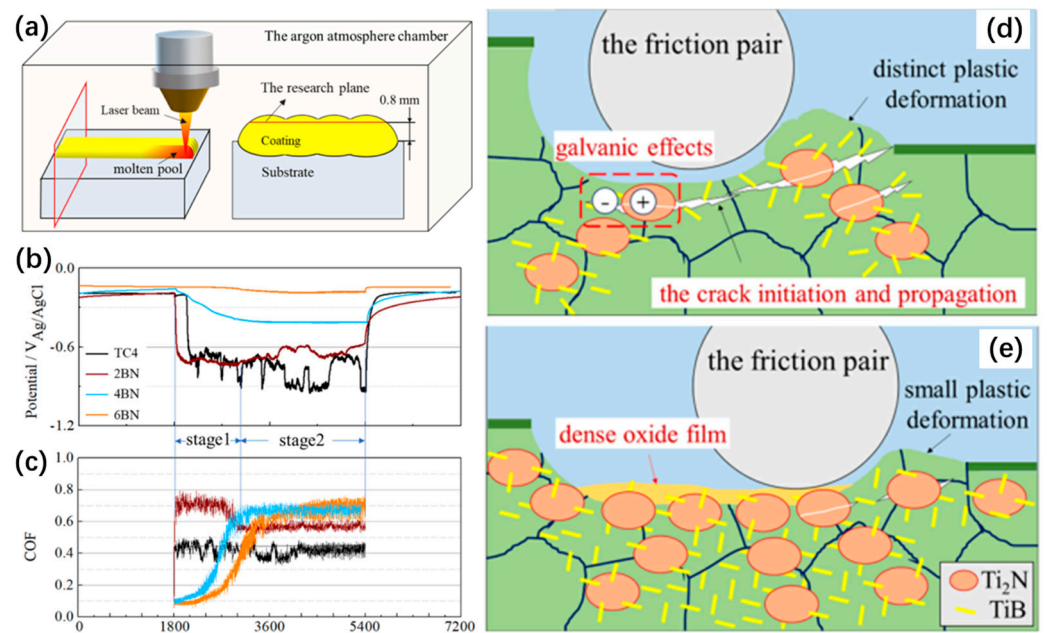


**Figure 15.** (a) The schematic of the laser cladding processes, (b) COF, and (c) OCP curves of TC4. Mechanism diagram of tribocorrosion process under the different conditions: (d) 2 BN, (e) 4 BN, and 6 BN coatings [163].

### 5.5. Duplex Treatment

There are many kinds of surface treatment technologies for titanium metal, each with its advantages and disadvantages. It is an inevitable trend to develop a variety of surface treatment technologies and synergistic protection for titanium metal parts used in extreme environments, such as nitriding, ion implantation, laser shock peening and vapor deposition coating composite technology, surface texturing and coating composite technology, micro-arc oxidation, and hybrid treatment technology [249,270–275]. Table 3 below shows some of the improvements in tribocorrosion of titanium alloys with duplex treatment.



**Table 3.** Some duplex treatment methods to improve the tribocorrosion resistance of titanium alloys.

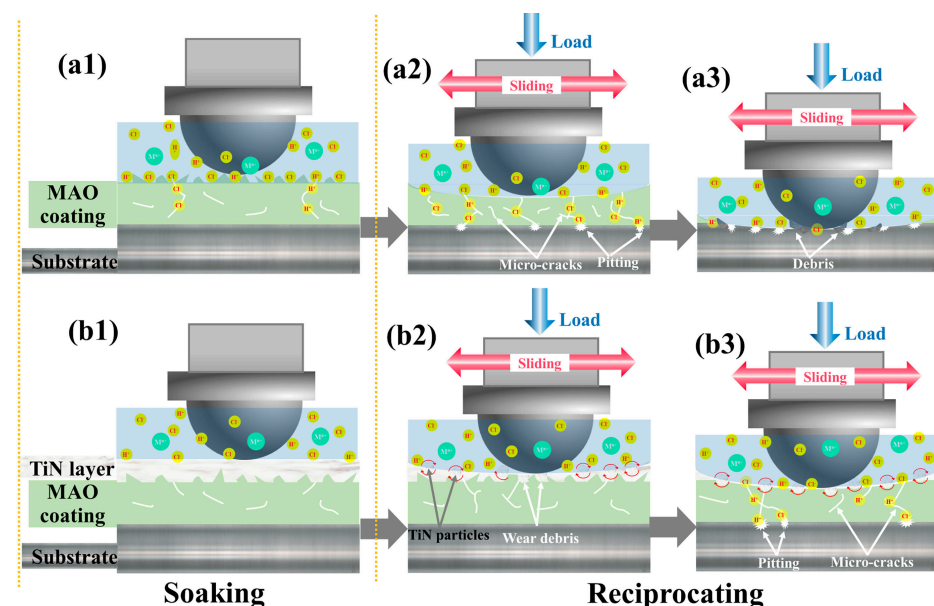
	Environment	Load [N]	Counterpart (Diameter) [mm]	Materials (Protective Layer)	Surface Treatment	OCP Values (V)	$E_{corr}$ (V)	$I_{corr}$ (A/cm <sup>2</sup> )	Friction Coefficient	Protective Layer Thickness [μm]	
<b>B. Cheraghali</b> [276]	PBS solution (Reference standards: ASTM F2129 America [277])	1.5	Al <sub>2</sub> O <sub>3</sub> [8 mm]	CP-Ti			−0.36	$7.5 \times 10^{-8}$	0.4		
				oxygen diffusion layers	thermal oxidation		−0.23	$2.9 \times 10^{-8}$	0.5	70 ± 5	
				TiO <sub>2</sub>	PEO, thermal oxidation		−0.03	$2.4 \times 10^{-9}$	0.4	2.3 ± 0.3	
<b>Erfan Abedi Esfahani</b> [278]	25% foetal bovine serum diluted in PBS electrolyte	5	Ti6Al4V [25 mm]	Ti6Al4V		−0.2	0.15	$1.5 \times 10^{-9}$			
			oxygen diffusion layers, TiN [25 mm]	oxygen diffusion layers, TiN	plasma oxidation, plasma nitriding, electron-beam plasma-assisted PVD	−0.1	−0.05	$6 \times 10^{-10}$	35~45 diffusion layer 3~6 TiN layer		
<b>Minpeng Dong</b> [279]	Seawater at 18 ± 3 °C	5	SiC [5 mm]	Ti6Al4V		−0.83	−0.58	$1.9 \times 10^{-5}$	0.38		
				TiSiCN	multi-arc ion plating		−0.02	−0.12	$1.1 \times 10^{-6}$	0.28	2.8
				TiSiCN, TiN, Ti <sub>2</sub> N	multi-arc ion plating + gas nitriding		0	−0.13	$1.7 \times 10^{-6}$	0.25	50 μm diffusion layers
<b>Chunlei Zhao</b> [280]	PBS solution (ASTM F2129)	2	SiC [6 mm]	Ti6Al4V		−0.8	−0.6	$2.4 \times 10^{-5}$	0.4~0.46		
				TiN	multi-arc ion plating		−0.05	−0.16	$1.1 \times 10^{-6}$	0.3~0.32	5.6
				TiN to embed TiO <sub>2</sub> nanotube coatings	multi-arc ion plating, electrochemical anodization		0.1	−0.02	$3 \times 10^{-7}$	0.18~0.26	5.6

Table 3. Cont.

Environment	Load [N]	Counterpart (Diameter) [mm]	Materials (Protective Layer)	Surface Treatment	OCP Values (V)	$E_{\text{corr}}$ (V)	$I_{\text{corr}}$ (A/cm <sup>2</sup> )	Friction Coefficient	Protective Layer Thickness [μm]
Jacek Grabarczyk [150]	PBS solution (ASTM F2129)	2	Al <sub>2</sub> O <sub>3</sub> [5 mm]	Ti6Al4V		−0.7		0.3~0.4	
				DLC layers	magnetron sputtering	−0.1		0.1	1~1.5 DLC layers
				oxygen compound layers	plasma oxidation	−0.7		0.4~0.7	
				oxygen compound layers, DLC layers	plasma oxidation, magnetron sputtering	0		0.1	1~1.5 DLC layers
				carbon compound layers	gas carburizing	−0.3		0.5~0.6	
				carbon compound layers, DLC layers	gas carburizing, magnetron sputtering	−0.3~−0.45		0.1~0.4	0.5~1.5 DLC layers

Kao et al. [281] showed that the duplex nitriding/TiN coating treatment significantly improved the tribological, anti-corrosion, and biocompatibility properties of the original Ti6Al4V alloy in 0.9 wt.% NaCl solution. Li et al. [279] investigated the TiSiCN/nitride duplex coatings prepared using gas nitriding and multi-arc ion plating. The effect of wear on corrosion was significant and the action of corrosion determined the total degree of synergy in the tribocorrosion system. Furthermore, the friction coefficient was greatly reduced through duplex coatings during the tribocorrosion test due to the good resistance to seawater and the graphitization effect produced by the TiSiCN layer. Zammit et al. [282] reported a two-phase treatment consisting of shot peening (SP) and physical vapor deposition (PVD) coatings to improve the surface properties of additive manufactured Ti-6Al-4V material. SP and duplex treatments resulted in a 13% and 210% increase in hardness, respectively. While untreated and SP-treated samples showed similar frictional corrosion behavior, the dual-treated samples showed the greatest resistance to corrosion wear, with no surface damage and a reduced rate of material loss.

Zhang et al. [283] prepared a dual-phase TiN-MAO coating on TC17 alloy using a hybrid treatment method combining MAO and high-power pulsed magnetron sputtering (HiPIMS). The corrosion and tribocorrosion properties of the bare substrate and coating substrate were comprehensively analyzed. The results of tribocorrosion showed that the synergistic effect of tribocorrosion lead to severe wear and adhesive wear of the bare substrate and MAO coating substrate. However, the dual-phase TiN-MAO coating exhibited the best tribocorrosion resistance, achieving the lowest CoF value (about 0.17) and wear rate (about  $6.21 \times 10^{-5} \text{ mm}^3 \cdot \text{N}^{-1} \cdot \text{m}^{-1}$ ) simultaneously under cathodic protection. The surface hardness of the dual-phase TiN-MAO coating was high, and only slight fracture and delamination occur on the wear scar. The irregular solid particles falling off the surface coating were trapped in the wear trajectory, resulting in third-body abrasive wear. The wear particles fell off and accumulated on the surface of the wear scar, playing the role of a rolling ball. The wear mechanism changed from sliding to rolling friction, significantly reducing the CoF. The corresponding friction mechanism is shown in Figure 16.



**Figure 16.** A schematic diagram for wear mechanism of the as-prepared coatings: (a1–a3) MAO-based coating, (b1–b3) duplex TiN-MAO coating [283].

The tribocorrosion behavior of a DLC coating system, as obtained by Hatem et al. [284], was investigated through a hybrid technique involving plasma immersion ion deposition (PIID) and plasma-enhanced magnetron sputtering (PEMS). The corresponding results can be seen in Figure 17. In PIID technology, the use of carbonaceous precursors (such as methane or acetylene) can produce DLC coatings with a very high hardness (10–25 GPa)

and a thickness of up to 2  $\mu\text{m}$ . Compared with other traditional technologies, the method is simpler and the cost is lower [285]. PEMS technology relies on the sputtering discharge of pure-carbon targets and the decomposition of hydrocarbons by electron impact of precursors [285]. Although PEMS can still deposit DLC, this technology is more suitable for producing carbide and nitride interlayers before DLC + PIID in biomedical coating systems. Therefore, the combination technique can be used to produce a DLC coating system with ideal tribocorrosion behavior because of the higher adhesion between the DLC, interlayer, and substrate. This technique was applied on Ti6Al4V alloy samples, specifically for biomedical applications. Compared with the Ti6Al4V bare alloy sample, the friction coefficient of the coating sample is reduced by at least five times, and the wear rate is less than 2%. The tribocorrosion behavior of DLC coatings prepared using PIID technology and PEMS + PIID technology is related to the mechanical properties and the formation of the carbon transfer layer, and the construction of the carbon transfer layer is closely related to the proportion of  $\text{sp}^2$  and  $\text{sp}^3$  bonds in the coating structure. The friction coefficient of the cyclic carbon transfer layer decreases along the reciprocating sliding test under PBS conditions, and the failure elastic strain of the DLC coating has a good correlation with the wear rate. The results show that the appropriate  $\text{sp}^2/\text{sp}^3$  bond fraction is crucial to the tribocorrosion properties of DLC coatings.

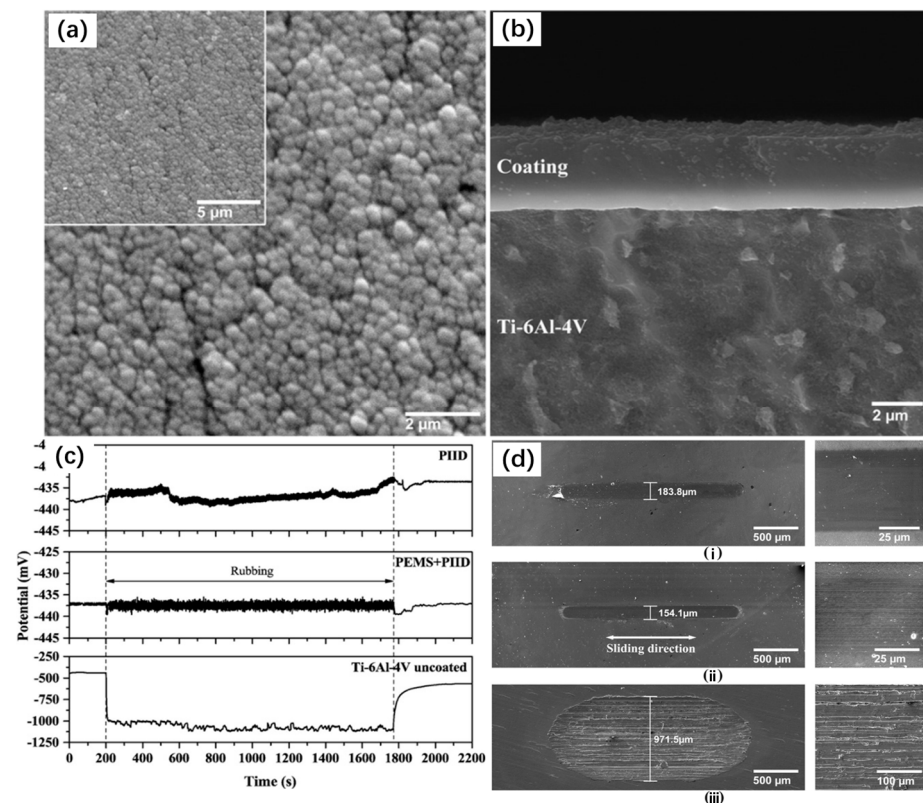


**Figure 17.** (a,b) Surface and cross-section SEM images by secondary electrons for the DLC coatings obtained with PEMS + PIID techniques, (c) OCP measurements before, during, and after tribocorrosion reciprocal sliding test in 1  $\times$  PBS solution for the PIID DLC coating, PEMS + PIID DLC coating, and Ti-6Al-4V uncoated samples, (d) SEM images of tribocorrosion wear tracks with measured width at left and center track enlarged at right for the (i) PIID DLC coating, (ii) PEMS + PIID DLC coating and (iii) Ti-6Al-4V uncoated samples [284].

Kong et al. [286] used a CrN interlayer to deposit a magnetron sputtering cr-diamond-like carbon (DLC) coating layer on a nitrated Ti6Al4V alloy (TAs) surface. Partial results are shown in Figure 18. The results showed that the Cr-DLC coating was an amorphous carbon (C) structure, and Cr clusters were dispersed in the Cr-DLC coating. The crystal structure

diagram was used to further analyze the bonding mechanism of the Cr-DLC coating at the interface. After nitriding treatment, some  $\alpha$ -Ti was transformed into  $\beta$ -Ti, increasing the TA's lattice density. The ionized nitrogen bombarded the surface of the nitrided TA to form a nitrided layer, and the dense TiN prevented C from penetrating the nitrided TA during the deposition of the Cr-DLC coating. The nitrided TA provided the load-bearing capacity for the Cr-DLC coating, reduced the hardness difference between the Cr-DLC coating and the nitrided TA, and improved its adhesion. The CrN interlayer connected the Cr-DLC coating with the nitrided TA, which enhanced the adhesion of the Cr-DLC coating at the interface. In this case, the CrN interlayer acted as a high-quality transition layer, which greatly solves the problem of poor adhesion between Cr-DLC and nitrided TA. The first-principles calculations have excellent application prospects for revealing the atomic-level theory of interface bonding.

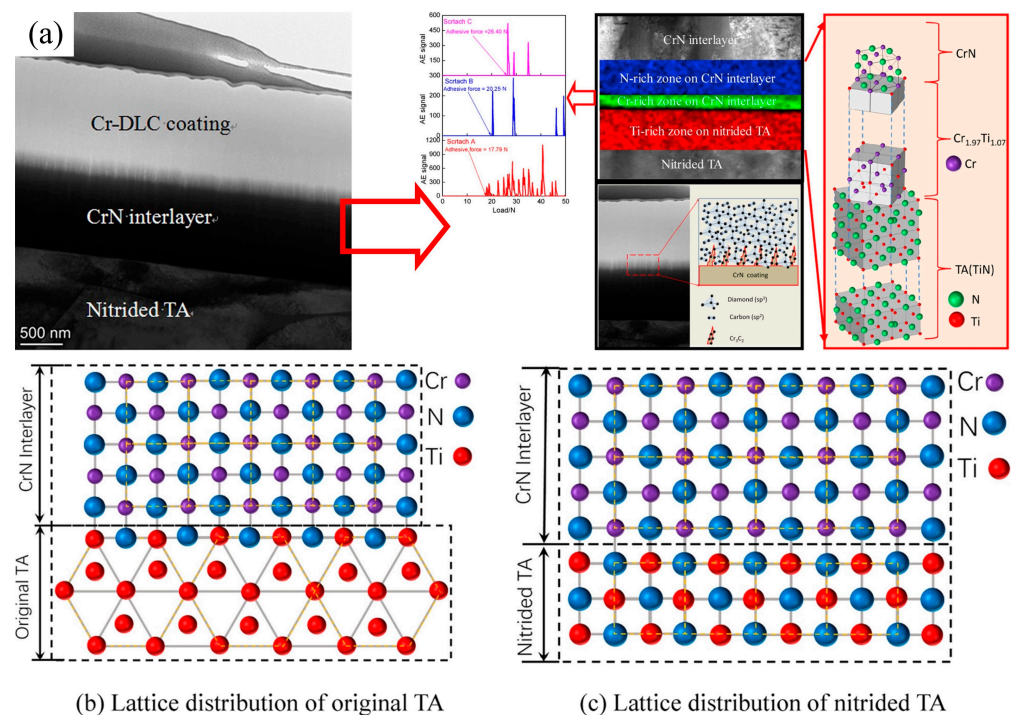


**Figure 18.** Models of crystal structure, lattice distributions, and adhesive force for the Cr-DLC coating–CrN interlayer–nitrided TA system: (a) Model of crystal structure, (b) Lattice distribution of original TA, (c) Lattice distribution of the nitrided TA [286].

## 6. Conclusions

In summary, corrosion wear is an essential factor affecting the application of titanium alloy structural materials in variable working conditions. At present, there are still many problems to be solved. There is a large gap between the simulated environment and the complex environment of the actual working conditions, and there are significant limitations in the theoretical guidance of engineering practice. As the equipment's service environment becomes more complex, the multi-factor coupling condition is more prominent. Given the existing problems of corrosion wear and surface strengthening protection of titanium alloy, the authors believe that conducting in-depth research on the following aspects is necessary.

- There are many factors affecting tribocorrosion. The interaction between corruption and wear cannot be superimposed by the loss caused by a single element. It is necessary to conduct damage evaluation device construction, evaluation method establishment, and research revealing the damage mechanism of titanium metal materials under extreme environments, complex working conditions, and multi-factor strong coupling.

- The traditional research and development system is mostly based on the ‘empirical design–experimental verification’ mode, and the composition and structural design of the auxiliary protective layer are less calculated based on molecular dynamics and first principles. The application of big data engineering, such as high-throughput computing and machine learning in coating research, development, and design, should be strengthened to fully explore the mapping relationship between the composition, organization, and performance of the coating. This will improve the design and development efficiency of high-performance protective layers.
- Traditional surface treatment technology has many technical difficulties that make it unsuitable for titanium metal treatment. A primary research direction is developing technology and equipment suitable for titanium metal surface treatment. The composite application of various surface treatment technologies, the design and preparation of multi-element, multilayer gradient structures, and ultra-thick surface modification layers meet the surface protection requirements of titanium metal in harsh environments.

**Author Contributions:** Writing—review and editing, Y.L.; Writing—original draft, Z.Z.; Supervision and revising manuscript, Y.H. All authors have read and agreed to the published version of the manuscript.

**Funding:** This research was funded by the National Natural Science Foundation of China, grant number 52175192.

**Data Availability Statement:** The data presented in this study are available on request from the corresponding author.

**Acknowledgments:** Thanks for the technical assistance from the state key laboratory of tribology in advanced equipment. We would like to express our heartfelt gratitude to Lu Jinpeng, Yan Jiwen, Dou Haichun, and Wang Zhengwei for their invaluable support in data collection.

**Conflicts of Interest:** The authors declare no conflict of interest.

## References

1. Muthaiah, V.M.S.; Indrakumar, S.; Suwas, S.; Chatterjee, K. Surface engineering of additively manufactured titanium alloys for enhanced clinical performance of biomedical implants: A review of recent developments. *Bioprinting* **2022**, *25*, e00180. [CrossRef]
2. Gao, A.; Hang, R.; Bai, L.; Tang, B.; Chu, P.K. Electrochemical surface engineering of titanium-based alloys for biomedical application. *Electrochim. Acta* **2018**, *271*, 699–718. [CrossRef]
3. Chourifa, H.; Bouloussa, H.; Migonney, V.; Falentin-Daudré, C. Review of titanium surface modification techniques and coatings for antibacterial applications. *Acta Biomater.* **2019**, *83*, 37–54. [CrossRef]
4. Gupta, M.K.; Etri, H.E.; Korkmaz, M.E.; Ross, N.S.; Krolczyk, G.M.; Gawlik, J.; Yaşar, N.; Pimenov, D.Y. Tribological and surface morphological characteristics of titanium alloys: A review. *Arch. Civ. Mech. Eng.* **2022**, *22*, 72. [CrossRef]
5. Li, G.; Chandra, S.; Rahman Rashid, R.A.; Palanisamy, S.; Ding, S. Machinability of additively manufactured titanium alloys: A comprehensive review. *J. Manuf. Process.* **2022**, *75*, 72–99. [CrossRef]
6. Kang, L.; Yang, C. A Review on High-Strength Titanium Alloys: Microstructure, Strengthening, and Properties. *Adv. Eng. Mater.* **2019**, *21*, 1801359. [CrossRef]
7. Ezugwu, E.O.; Wang, Z.M. Titanium alloys and their machinability—A review. *J. Mater. Process. Technol.* **1997**, *68*, 262–274. [CrossRef]
8. Hourmand, M.; Sarhan, A.A.D.; Sayuti, M.; Hamdi, M. A Comprehensive Review on Machining of Titanium Alloys. *Arab. J. Sci. Eng.* **2021**, *46*, 7087–7123. [CrossRef]
9. Pasang, T.; Budiman, A.S.; Wang, J.C.; Jiang, C.P.; Boyer, R.; Williams, J.; Misiolak, W.Z. Additive manufacturing of titanium alloys—Enabling re-manufacturing of aerospace and biomedical components. *Microelectron. Eng.* **2023**, *270*, 111935. [CrossRef]
10. Yue, D.; Jiang, X.; Yu, H.; Sun, D. In-situ fabricated hierarchical nanostructure on titanium alloy as highly stable and durable super-lubricated surface for anti-biofouling in marine engineering. *Chem. Eng. J.* **2023**, *463*, 142389. [CrossRef]
11. Gummadi, J.; Alanka, S. A review on titanium and titanium alloys with other metals for biomedical applications prepared by powder metallurgy techniques. *Mater. Today Proc.* **2023**, *in press*. [CrossRef]
12. Zhao, Q.; Sun, Q.; Xin, S.; Chen, Y.; Wu, C.; Wang, H.; Xu, J.; Wan, M.; Zeng, W.; Zhao, Y. High-strength titanium alloys for aerospace engineering applications: A review on melting-forging process. *Mater. Sci. Eng. A* **2022**, *845*, 143260. [CrossRef]
13. Gurrappa, I. Characterization of titanium alloy Ti-6Al-4V for chemical, marine and industrial applications. *Mater. Charact.* **2003**, *51*, 131–139. [CrossRef]

14. Zhang, W.; Fan, J.; Huang, H.; Xue, X.; Wang, Y.; Zhang, B.; Jiang, P.; Wang, C.; Kou, H.; Li, J. Creep anisotropy characteristics and microstructural crystallography of marine engineering titanium alloy Ti6321 plate at room temperature. *Mater. Sci. Eng. A* **2022**, *854*, 143728. [[CrossRef](#)]
15. Kappenthuler, S.; Seeger, S. Holistic evaluation of the suitability of metal alloys for sustainable marine construction from a technical, economic and availability perspective. *Ocean Eng.* **2021**, *219*, 108378. [[CrossRef](#)]
16. Nichul, U.; Hiwarkar, V. Carbon dot complimentary green corrosion inhibitor for crystallographically textured Beta C titanium alloy for marine application: A state of art. *J. Alloys Compd.* **2023**, *962*, 171116. [[CrossRef](#)]
17. Leonov, V.P.; Mikhaylov, V.I. Technological and constructional features of welding titanium alloys for marine structures. *Weld. Int.* **2016**, *30*, 403–407. [[CrossRef](#)]
18. Lee Williams, W. Development of structural titanium alloys for marine applications. *Ocean Eng.* **1969**, *1*, 375–383. [[CrossRef](#)]
19. Li, J.; Zhang, D.; Chen, X.; Xu, D.; Qiu, D.; Wang, F.; Easton, M. Laser directed energy deposited, ultrafine-grained functional titanium-copper alloys tailored for marine environments: Antibacterial and anti-microbial corrosion studies. *J. Mater. Sci. Technol.* **2023**, *166*, 21–33. [[CrossRef](#)]
20. Sánchez, N.A.; Rincón, C.; Zambrano, G.; Galindo, H.; Prieto, P. Characterization of diamond-like carbon (DLC) thin films prepared by r.f. magnetron sputtering. *Thin Solid Film.* **2000**, *373*, 247–250. [[CrossRef](#)]
21. Ulusaloğlu, A.C.; Atici, T.; Ermutlu, C.; Akesen, S. Evaluation of titanium release from titanium alloy implants in patients with spinal instrumentation. *J. Int. Med. Res.* **2021**, *49*, 0300060520984931. [[CrossRef](#)] [[PubMed](#)]
22. Liu, X.; Chen, S.; Tsoi, J.K.H.; Matinlinna, J.P. Binary titanium alloys as dental implant materials—A review. *Regen. Biomater.* **2017**, *4*, 315–323. [[CrossRef](#)] [[PubMed](#)]
23. Grigoriev, S.; Sotova, C.; Vereschaka, A.; Uglov, V.; Cherenda, N. Modifying Coatings for Medical Implants Made of Titanium Alloys. *Metals* **2023**, *13*, 718. [[CrossRef](#)]
24. Zhang, S.; Yu, Y.; Wang, H.; Ren, L.; Yang, K. Study on mechanical behavior of Cu-bearing antibacterial titanium alloy implant. *J. Mech. Behav. Biomed. Mater.* **2022**, *125*, 104926. [[CrossRef](#)] [[PubMed](#)]
25. Cordeiro, J.M.; Beline, T.; Ribeiro, A.L.R.; Rangel, E.C.; da Cruz, N.C.; Landers, R.; Faverani, L.P.; Vaz, L.G.; Fais, L.M.G.; Vicente, F.B.; et al. Development of binary and ternary titanium alloys for dental implants. *Dent. Mater.* **2017**, *33*, 1244–1257. [[CrossRef](#)] [[PubMed](#)]
26. Jin, B.; Wang, Q.; Zhao, L.; Pan, A.; Ding, X.; Gao, W.; Song, Y.; Zhang, X. A Review of Additive Manufacturing Techniques and Post-Processing for High-Temperature Titanium Alloys. *Metals* **2023**, *13*, 1327. [[CrossRef](#)]
27. Chowdhury, S.; Arunachalam, N. Surface functionalization of additively manufactured titanium alloy for orthopaedic implant applications. *J. Manuf. Process.* **2023**, *102*, 387–405. [[CrossRef](#)]
28. Alipour, S.; Moridi, A.; Liou, F.; Emdadi, A. The Trajectory of Additively Manufactured Titanium Alloys with Superior Mechanical Properties and Engineered Microstructures. *Addit. Manuf.* **2022**, *60*, 103245. [[CrossRef](#)]
29. Trevisan, F.; Calignano, F.; Aversa, A.; Marchese, G.; Lombardi, M.; Biamino, S.; Ugues, D.; Manfredi, D. Additive manufacturing of titanium alloys in the biomedical field: Processes, properties and applications. *J. Appl. Biomater. Funct. Mater.* **2017**, *16*, 57–67. [[CrossRef](#)]
30. Zhang, L.-C.; Liu, Y.; Li, S.; Hao, Y. Additive Manufacturing of Titanium Alloys by Electron Beam Melting: A Review. *Adv. Eng. Mater.* **2018**, *20*, 1700842. [[CrossRef](#)]
31. Wang, B.; Lan, J.; Qiao, H.; Xie, L.; Yang, H.; Lin, H.; Li, X.; Huang, Y. Porous surface with fusion peptides embedded in strontium titanate nanotubes elevates osteogenic and antibacterial activity of additively manufactured titanium alloy. *Colloids Surf. B Biointerfaces* **2023**, *224*, 113188. [[CrossRef](#)] [[PubMed](#)]
32. Kwak, T.Y.; Yang, J.Y.; Heo, Y.B.; Kim, S.J.; Kwon, S.Y.; Kim, W.J.; Lim, D.H. Additive manufacturing of a porous titanium layer structure Ti on a Co–Cr alloy for manufacturing cementless implants. *J. Mater. Res. Technol.* **2021**, *10*, 250–267. [[CrossRef](#)]
33. Xu, J.; Lu, Y.; Pan, X.; Zhan, D.; Wang, Q.; Zhang, N. Antibacterial performance of a porous Cu-bearing titanium alloy by laser additive manufacturing. *Front. Bioeng. Biotechnol.* **2023**, *11*, 1226745. [[CrossRef](#)] [[PubMed](#)]
34. Kaur, M.; Singh, K. Review on titanium and titanium based alloys as biomaterials for orthopaedic applications. *Mater. Sci. Eng. C* **2019**, *102*, 844–862. [[CrossRef](#)] [[PubMed](#)]
35. Yan, Y.; Zhang, Y.; Wang, Q.; Du, H.; Qiao, L. Effect of povidone–iodine deposition on tribocorrosion and antibacterial properties of titanium alloy. *Appl. Surf. Sci.* **2016**, *363*, 432–438. [[CrossRef](#)]
36. Pejaković, V.; Berger, L.-M.; Thiele, S.; Rojacz, H.; Rodríguez Ripoll, M. Fine grained titanium carbonitride reinforcements for laser deposition processes of 316L boost tribocorrosion resistance in marine environments. *Mater. Des.* **2021**, *207*, 109847. [[CrossRef](#)]
37. Feng, J.; Xiao, H. Tribocorrosion Behavior of Laser Cladded Ti–Al–(C, N) Composite Coatings in Artificial Seawater. *Coatings* **2022**, *12*, 187. [[CrossRef](#)]
38. Peacock, D.K.; Corr, M.I. Effective Design of High Performance Corrosion Resistant Systems For Oceanic Environments Using Titanium. *Corros. Rev.* **2000**, *18*, 295–330. [[CrossRef](#)]
39. Cui, N.; Chen, S.; Xu, T.; Sun, W.; Lv, B.; Zhang, S.; Niu, H.; Kong, F. The Microstructure, Mechanical Properties, and Corrosion Resistance of a Novel Extruded Titanium Alloy. *Metals* **2022**, *12*, 1564. [[CrossRef](#)]
40. Li, Z.; Wang, J.; Dong, Y.; Xu, D.; Zhang, X.; Wu, J.; Gu, T.; Wang, F. Synergistic effect of chloride ion and *Shewanella* algae accelerates the corrosion of Ti-6Al-4V alloy. *J. Mater. Sci. Technol.* **2021**, *71*, 177–185. [[CrossRef](#)]

41. Chen, W.; Li, R.; Liu, L.; Liu, R.; Cui, Y.; Chen, Z.; Wang, Q.; Wang, F. Effect of NaCl-rich environment on internal corrosion for Ti60 alloy at 600 °C. *Corros. Sci.* **2023**, *220*, 111307. [[CrossRef](#)]
42. Prando, D.; Brenna, A.; Diamanti, M.V.; Beretta, S.; Bolzoni, F.; Ormellese, M.; Pedeferra, M. Corrosion of Titanium: Part 1: Aggressive Environments and Main Forms of Degradation. *J. Appl. Biomater. Funct. Mater.* **2017**, *15*, e291–e302. [[CrossRef](#)] [[PubMed](#)]
43. Oryshchenko, A.S.; Gorynin, I.V.; Leonov, V.P.; Kudryavtsev, A.S.; Mikhailov, V.I.; Chudakov, E.V. Marine titanium alloys: Present and future. *Inorg. Mater. Appl. Res.* **2015**, *6*, 571–579. [[CrossRef](#)]
44. Jáquez-Muñoz, J.M.; Gaona-Tiburcio, C.; Cabral-Miramontes, J.; Nieves-Mendoza, D.; Maldonado-Bandala, E.; Olguín-Coca, J.; López-Léon, L.D.; Flores-De los Rios, J.P.; Almeraya-Calderón, F. Electrochemical Noise Analysis of the Corrosion of Titanium Alloys in NaCl and H<sub>2</sub>SO<sub>4</sub> Solutions. *Metals* **2021**, *11*, 105. [[CrossRef](#)]
45. Pejaković, V.; Totolin, V.; Rodríguez Ripoll, M. Tribocorrosion behaviour of Ti6Al4V in artificial seawater at low contact pressures. *Tribol. Int.* **2018**, *119*, 55–65. [[CrossRef](#)]
46. Ferreira, D.F.; Almeida, S.M.A.; Soares, R.B.; Juliani, L.; Bracarense, A.Q.; Lins, V.d.F.C.; Junqueira, R.M.R. Synergism between mechanical wear and corrosion on tribocorrosion of a titanium alloy in a Ringer solution. *J. Mater. Res. Technol.* **2019**, *8*, 1593–1600. [[CrossRef](#)]
47. Licausi, M.P.; Igual Muñoz, A.; Amigó Borrás, V. Influence of the fabrication process and fluoride content on the tribocorrosion behaviour of Ti6Al4V biomedical alloy in artificial saliva. *J. Mech. Behav. Biomed. Mater.* **2013**, *20*, 137–148. [[CrossRef](#)]
48. Brune, D.A.G.; Evje, D.A.G.; Melsom, S. Corrosion of gold alloys and titanium in artificial saliva. *Eur. J. Oral Sci.* **1982**, *90*, 168–171. [[CrossRef](#)]
49. Hacisalihoglu, I.; Samancioglu, A.; Yildiz, F.; Purcek, G.; Alasaran, A. Tribocorrosion properties of different type titanium alloys in simulated body fluid. *Wear* **2015**, *332–333*, 679–686. [[CrossRef](#)]
50. Kassapidou, M.; Hjalmarsson, L.; Johansson, C.B.; Hammarström Johansson, P.; Morisbak, E.; Wennerberg, A.; Franke Stenport, V. Cobalt–chromium alloys fabricated with four different techniques: Ion release, toxicity of released elements and surface roughness. *Dent. Mater.* **2020**, *36*, e352–e363. [[CrossRef](#)]
51. Saldaña, L.; Barranco, V.; García-Alonso, M.C.; Vallés, G.; Escudero, M.L.; Munuera, L.; Vilaboa, N. Concentration-dependent effects of titanium and aluminium ions released from thermally oxidized Ti6Al4V alloy on human osteoblasts. *J. Biomed. Mater. Res. Part A* **2006**, *77A*, 220–229. [[CrossRef](#)] [[PubMed](#)]
52. Noubissi, S.; Scarano, A.; Gupta, S. A Literature Review Study on Atomic Ions Dissolution of Titanium and Its Alloys in Implant Dentistry. *Materials* **2019**, *12*, 368. [[CrossRef](#)]
53. Balachandran, S.; Zachariah, Z.; Fischer, A.; Mayweg, D.; Wimmer, M.A.; Raabe, D.; Herbig, M. Metallic Implants: Atomic Scale Origin of Metal Ion Release from Hip Implant Taper Junctions (Adv. Sci. 5/2020). *Adv. Sci.* **2020**, *7*, 2070027. [[CrossRef](#)]
54. Ortiz, A.J.; Fernández, E.; Vicente, A.; Calvo, J.L.; Ortiz, C. Metallic ions released from stainless steel, nickel-free, and titanium orthodontic alloys: Toxicity and DNA damage. *Am. J. Orthod. Dentofac. Orthop.* **2011**, *140*, e115–e122. [[CrossRef](#)] [[PubMed](#)]
55. Marian, M.; Berman, D.; Nečas, D.; Emami, N.; Ruggiero, A.; Rosenkranz, A. Roadmap for 2D materials in biotribological/biomedical applications—A review. *Adv. Colloid Interface Sci.* **2022**, *307*, 102747. [[CrossRef](#)]
56. Deng, Y.; Chen, W.; Li, B.; Wang, C.; Kuang, T.; Li, Y. Physical vapor deposition technology for coated cutting tools: A review. *Ceram. Int.* **2020**, *46*, 18373–18390. [[CrossRef](#)]
57. Zheng, Y.; Xu, P. Effect of Nb Content on Phase Transformation and Comprehensive Properties of TiNb Alloy Coating. *Coatings* **2023**, *13*, 1186. [[CrossRef](#)]
58. Chang, S.-H.; Tang, T.-C.; Huang, K.-T.; Liu, C.-M. Investigation of the characteristics of DLC films on oxynitriding-treated ASP23 high speed steel by DC-pulsed PECVD process. *Surf. Coat. Technol.* **2015**, *261*, 331–336. [[CrossRef](#)]
59. Täfner, U.C.V.; Schäfer, U.; Handbook, A.S.M. *Metallography and Microstructures*; ASM International Materials Park: Novelty, OH, USA, 2004; Volume 9.
60. Ribeiro, M.V.; Moreira, M.R.V.; Ferreira, J.R. Optimization of titanium alloy (6Al–4V) machining. *J. Mater. Process. Technol.* **2003**, *143–144*, 458–463. [[CrossRef](#)]
61. Balachandran, S.; Mishra, R.S.; Banerjee, D. Friction stir processing of a metastable  $\beta$  titanium alloy in  $\beta$  and  $\alpha + \beta$  phase fields. *Mater. Sci. Eng. A* **2020**, *772*, 138705. [[CrossRef](#)]
62. Zhou, L.; Sun, J.; Zhang, R.; Chen, J.; He, J.; Yuan, T. A new insight into the  $\alpha$  phase precipitation in  $\beta$  titanium alloy. *Vacuum* **2021**, *189*, 110272. [[CrossRef](#)]
63. Dash, B.; Jangid, R.; Koneru, S.R.; Pilchak, A.; Banerjee, D. The formation of  $\alpha$  at triple junctions of parent  $\beta$  phase in titanium alloys. *Philos. Mag.* **2019**, *99*, 956–970. [[CrossRef](#)]
64. Dong, R.; Kou, H.; Wu, L.; Yang, L.; Zhao, Y.; Hou, H.  $\beta$  to  $\omega$  transformation strain associated with the precipitation of  $\alpha$  phase in a metastable  $\beta$  titanium alloy. *J. Mater. Sci.* **2021**, *56*, 1685–1693. [[CrossRef](#)]
65. Zhu, C.; Zhang, X.-Y.; Li, C.; Liu, C.; Zhou, K. A strengthening strategy for metastable  $\beta$  titanium alloys: Synergy effect of primary  $\alpha$  phase and  $\beta$  phase stability. *Mater. Sci. Eng. A* **2022**, *852*, 143736. [[CrossRef](#)]
66. Markovskiy, P.E.; Bondarchuk, V.I. Influence of Strain Rate, Microstructure and Chemical and Phase Composition on Mechanical Behavior of Different Titanium Alloys. *J. Mater. Eng. Perform.* **2017**, *26*, 3431–3449. [[CrossRef](#)]
67. Illarionov, A.G.; Nezhdanov, A.G.; Stepanov, S.I.; Muller-Kamskii, G.; Popov, A.A. Structure, Phase Composition, and Mechanical Properties of Biocompatible Titanium Alloys of Different Types. *Phys. Met. Metallogr.* **2020**, *121*, 367–373. [[CrossRef](#)]



68. Zheng, Y.; Williams, R.E.A.; Nag, S.; Banerjee, R.; Fraser, H.L.; Banerjee, D. The effect of alloy composition on instabilities in the  $\beta$  phase of titanium alloys. *Scr. Mater.* **2016**, *116*, 49–52. [[CrossRef](#)]
69. Liu, C.; Li, G.; Yuan, F.; Ali, M.; Han, F.; Zhang, Y.; Gu, H. Oxygen induced phase transformation in an  $\alpha + \beta$  titanium alloy. *Mater. Chem. Phys.* **2019**, *223*, 75–77. [[CrossRef](#)]
70. Cao, S.; Mischler, S. Modeling tribocorrosion of passive metals—A review. *Curr. Opin. Solid State Mater. Sci.* **2018**, *22*, 127–141. [[CrossRef](#)]
71. Xiao, J.-K.; Xu, G.-M.; Chen, J.; Rusinov, P.; Zhang, C. Tribocorrosion behavior of TiZrHfNb-based refractory high-entropy alloys. *Wear* **2024**, 536–537, 205158. [[CrossRef](#)]
72. Liu, H.; Huang, X.; Huang, S.; Qiao, L.; Yan, Y. Anisotropy of wear and tribocorrosion properties of L-PBF Ti6Al4V. *J. Mater. Res. Technol.* **2023**, *25*, 2690–2701. [[CrossRef](#)]
73. Wood, R.J.K. Marine wear and tribocorrosion. *Wear* **2017**, 376–377, 893–910. [[CrossRef](#)]
74. Yan, C.; Zeng, Q.; Xu, Y.; He, W. Microstructure, phase and tribocorrosion behavior of 60NiTi alloy. *Appl. Surf. Sci.* **2019**, *498*, 143838. [[CrossRef](#)]
75. Correa, D.R.N.; Kuroda, P.A.B.; Grandini, C.R.; Rocha, L.A.; Oliveira, F.G.M.; Alves, A.C.; Toptan, F. Tribocorrosion behavior of  $\beta$ -type Ti-15Zr-based alloys. *Mater. Lett.* **2016**, *179*, 118–121. [[CrossRef](#)]
76. Wang, W.; Wang, K.; Zhang, Z.; Chen, J.; Mou, T.; Michel, F.M.; Xin, H.; Cai, W. Ultrahigh tribocorrosion resistance of metals enabled by nano-layering. *Acta Mater.* **2021**, *206*, 116609. [[CrossRef](#)]
77. De Stefano, M.; Aliberti, S.M.; Ruggiero, A. (Bio)Tribocorrosion in Dental Implants: Principles and Techniques of Investigation. *Appl. Sci.* **2022**, *12*, 7421. [[CrossRef](#)]
78. Li, Z.; Yu, H.; Sun, D. The tribocorrosion mechanism of aluminum alloy 7075-T6 in the deep ocean. *Corros. Sci.* **2021**, *183*, 109306. [[CrossRef](#)]
79. Kosec, T.; Močnik, P.; Legat, A. The tribocorrosion behaviour of NiTi alloy. *Appl. Surf. Sci.* **2014**, *288*, 727–735. [[CrossRef](#)]
80. Lei, M.K.; Ou, Y.X.; Wang, K.S.; Chen, L. Wear and corrosion properties of plasma-based low-energy nitrogen ion implanted titanium. *Surf. Coat. Technol.* **2011**, *205*, 4602–4607. [[CrossRef](#)]
81. Sato, J.; Shima, M.; Takeuchi, M. Fretting wear in seawater. *Wear* **1986**, *110*, 227–238. [[CrossRef](#)]
82. Soares, C.G.; Garbatov, Y.; Zayed, A.; Wang, G. Influence of environmental factors on corrosion of ship structures in marine atmosphere. *Corros. Sci.* **2009**, *51*, 2014–2026. [[CrossRef](#)]
83. Noël, R.E.J.; Ball, A. On the synergistic effects of abrasion and corrosion during wear. *Wear* **1983**, *87*, 351–361. [[CrossRef](#)]
84. Jiang, X. Progress in Research on Wear-corrosion. *Mater. Rev.* **2001**, *15*, 20–22.
85. Sinnett-Jones, P.E.; Wharton, J.A.; Wood, R.J.K. Micro-abrasion–corrosion of a CoCrMo alloy in simulated artificial hip joint environments. *Wear* **2005**, *259*, 898–909. [[CrossRef](#)]
86. Mathew, M.T.; Srinivasa Pai, P.; Pourzal, R.; Fischer, A.; Wimmer, M.A. Significance of Tribocorrosion in Biomedical Applications: Overview and Current Status. *Adv. Tribol.* **2009**, *2009*, 250986. [[CrossRef](#)]
87. Mace, A.; Gilbert, J.L. A mass balance analysis of the tribocorrosion process of titanium alloys using a single micro-asperity: Voltage and solution effects on plastic deformation, oxide repassivation, and ion dissolution. *J. Mech. Behav. Biomed. Mater.* **2022**, *136*, 105531. [[CrossRef](#)] [[PubMed](#)]
88. Mathew, M.T.; Barão, V.A.; Yuan, J.C.-C.; Assunção, W.G.; Sukotjo, C.; Wimmer, M.A. What is the role of lipopolysaccharide on the tribocorrosive behavior of titanium? *J. Mech. Behav. Biomed. Mater.* **2012**, *8*, 71–85. [[CrossRef](#)]
89. Tan, L.; Wang, Z.; Ma, Y.; Yan, Y.; Qiao, L. Tribocorrosion investigation of 316L stainless steel: The synergistic effect between chloride ion and sulfate ion. *Mater. Res. Express* **2021**, *8*, 086501. [[CrossRef](#)]
90. Liu, Y.; Liu, L.; Li, S.; Wang, R.; Guo, P.; Wang, A.; Ke, P. Accelerated deterioration mechanism of 316L stainless steel in NaCl solution under the intermittent tribocorrosion process. *J. Mater. Sci. Technol.* **2022**, *121*, 67–79. [[CrossRef](#)]
91. López-Ortega, A.; Bayón, R.; Arana, J.L.; Arredondo, A.; Igartua, A. Influence of temperature on the corrosion and tribocorrosion behaviour of High-Strength Low-Alloy steels used in offshore applications. *Tribol. Int.* **2018**, *121*, 341–352. [[CrossRef](#)]
92. Pu, J.; Zhang, Y.; Zhang, X.; Yuan, X.; Ren, P.; Jin, Z. Mapping the fretting corrosion behaviors of 6082 aluminum alloy in 3.5% NaCl solution. *Wear* **2021**, *482*, 203975. [[CrossRef](#)]
93. Chen, J.; Zhang, Q. Effect of electrochemical state on corrosion–wear behaviors of TC4 alloy in artificial seawater. *Trans. Nonferrous Met. Soc. China* **2016**, *26*, 1011–1018. [[CrossRef](#)]
94. Ding, H.; Dai, Z.; Xu, T. Fretting Wear Mechanism of Titanium in Water. *Lubr. Eng.* **2005**, *6*, 28–29+32.
95. Xu, Y.; Qi, J.; Nutter, J.; Sharp, J.; Bai, M.; Ma, L.; Rainforth, W.M. Correlation between the formation of tribofilm and repassivation in biomedical titanium alloys during tribocorrosion. *Tribol. Int.* **2021**, *163*, 107147. [[CrossRef](#)]
96. Zhao, Q.; Ueno, T.; Wakabayashi, N. A review in titanium-zirconium binary alloy for use in dental implants: Is there an ideal Ti-Zr composing ratio? *Jpn. Dent. Sci. Rev.* **2023**, *59*, 28–37. [[CrossRef](#)] [[PubMed](#)]
97. Siony, N.; Vuong, L.; Lundaajamts, O.; Kadkhodaei, S. Computational design of corrosion-resistant and wear-resistant titanium alloys for orthopedic implants. *Mater. Today Commun.* **2022**, *33*, 104465. [[CrossRef](#)]
98. Shah, S.D.; Zheng, F.; Seghi, R.R.; Lee, D.J. Strength of titanium-zirconium alloy implants with a conical connection after implantoplasty. *J. Prosthet. Dent.* **2022**, *in press*. [[CrossRef](#)]
99. Afzali, P.; Ghomashchi, R.; Oskouei, R.H. On the Corrosion Behaviour of Low Modulus Titanium Alloys for Medical Implant Applications: A Review. *Metals* **2019**, *9*, 878. [[CrossRef](#)]

100. Bédouin, Y.; Gordin, D.-M.; Pellen-Mussi, P.; Pérez, F.; Tricot-Doleux, S.; Vasilescu, C.; Drob, S.I.; Chauvel-Lebret, D.; Gloriant, T. Enhancement of the biocompatibility by surface nitriding of a low-modulus titanium alloy for dental implant applications. *J. Biomed. Mater. Res. Part B Appl. Biomater.* **2019**, *107*, 1483–1490. [[CrossRef](#)]
101. Gibson, L.J. Cellular Solids. *MRS Bull.* **2003**, *28*, 270–274. [[CrossRef](#)]
102. Wauthle, R.; Vrancken, B.; Beynaerts, B.; Jorissen, K.; Schrooten, J.; Kruth, J.-P.; Van Humbeeck, J. Effects of build orientation and heat treatment on the microstructure and mechanical properties of selective laser melted Ti6Al4V lattice structures. *Addit. Manuf.* **2015**, *5*, 77–84. [[CrossRef](#)]
103. Guo, S.; Meng, Q.; Zhao, X.; Wei, Q.; Xu, H. Design and fabrication of a metastable  $\beta$ -type titanium alloy with ultralow elastic modulus and high strength. *Sci. Rep.* **2015**, *5*, 14688. [[CrossRef](#)]
104. Xiang, T.; Chen, J.; Bao, W.; Zhong, S.; Du, P.; Xie, G. Fabrication of porous TiZrNbTa high-entropy alloys/Ti composite with high strength and low Young's modulus using a novel MgO space holder. *J. Mater. Sci. Technol.* **2023**, *167*, 59–73. [[CrossRef](#)]
105. Li, S.; Lee, W.-T.; Yeom, J.-T.; Kim, J.G.; Oh, J.S.; Lee, T.; Liu, Y.; Nam, T.-H. Towards bone-like elastic modulus in TiNbSn alloys with large recovery strain for biomedical applications. *J. Alloys Compd.* **2022**, *925*, 166724. [[CrossRef](#)]
106. Krishna, B.V.; Bose, S.; Bandyopadhyay, A. Low stiffness porous Ti structures for load-bearing implants. *Acta Biomater.* **2007**, *3*, 997–1006. [[CrossRef](#)] [[PubMed](#)]
107. Kang, B.; Chen, X.; Liu, P. Facile fabrication of nanoporous structure on  $\beta$  titanium alloy to eliminate stress shielding for bone implant. *J. Vac. Sci. Technol. B* **2022**, *40*, 050601. [[CrossRef](#)]
108. Arias-González, F.; Rodríguez-Contreras, A.; Punset, M.; Manero, J.M.; Barro, Ó.; Fernández-Arias, M.; Lusquiños, F.; Gil, J.; Pou, J. Laser-Deposited Beta Type Ti-42Nb Alloy with Anisotropic Mechanical Properties for Pioneering Biomedical Implants with a Very Low Elastic Modulus. *Materials* **2022**, *15*, 7172. [[CrossRef](#)]
109. Cai, D.; Zhao, X.; Yang, L.; Wang, R.; Qin, G.; Chen, D.-f.; Zhang, E. A novel biomedical titanium alloy with high antibacterial property and low elastic modulus. *J. Mater. Sci. Technol.* **2021**, *81*, 13–25. [[CrossRef](#)]
110. Ito, K.; Mori, Y.; Kamimura, M.; Koguchi, M.; Kurishima, H.; Koyama, T.; Mori, N.; Masahashi, N.; Hanada, S.; Itoi, E.; et al.  $\beta$ -type TiNbSn Alloy Plates with Low Young Modulus Accelerates Osteosynthesis in Rabbit Tibiae. *Clin. Orthop. Relat. Res.* **2022**, *480*, 1817–1832. [[CrossRef](#)]
111. Singh, D.; Garg, B.; Pandey, P.M.; Kalyanasundaram, D. Design and development of 3D printing assisted microwave sintering of elbow implant with biomechanical properties similar to human elbow. *Rapid Prototyp. J.* **2022**, *28*, 390–403. [[CrossRef](#)]
112. Gao, X.; Zhao, Y.; Wang, M.; Liu, Z.; Liu, C. Parametric Design of Hip Implant With Gradient Porous Structure. *Front. Bioeng. Biotechnol.* **2022**, *10*, 850184. [[CrossRef](#)]
113. Li, Y.; Yang, C.; Zhao, H.; Qu, S.; Li, X.; Li, Y. New Developments of Ti-Based Alloys for Biomedical Applications. *Materials* **2014**, *7*, 1709–1800. [[CrossRef](#)]
114. Song, C.; Liu, L.; Deng, Z.; Lei, H.; Yuan, F.; Yang, Y.; Li, Y.; Jiakuo, Y. Research progress on the design and performance of porous titanium alloy bone implants. *J. Mater. Res. Technol.* **2023**, *23*, 2626–2641. [[CrossRef](#)]
115. Guo, A.X.Y.; Cheng, L.; Zhan, S.; Zhang, S.; Xiong, W.; Wang, Z.; Wang, G.; Cao, S.C. Biomedical applications of the powder-based 3D printed titanium alloys: A review. *J. Mater. Sci. Technol.* **2022**, *125*, 252–264. [[CrossRef](#)]
116. Kostornov, A.G.; Akhmedov, M.K. Physicomechanical properties of porous materials of VT6 titanium alloy fibers. *Powder Metall. Met. Ceram.* **1995**, *33*, 426–430. [[CrossRef](#)]
117. Bai, X.; Li, J.; Zhao, Z.; Wang, Q.; Lv, N.; Wang, Y.; Gao, H.; Guo, Z.; Li, Z. In vivo evaluation of osseointegration ability of sintered bionic trabecular porous titanium alloy as artificial hip prosthesis. *Front. Bioeng. Biotechnol.* **2022**, *10*, 928216. [[CrossRef](#)]
118. Wang, R.; Ni, S.; Ma, L.; Li, M. Porous construction and surface modification of titanium-based materials for osteogenesis: A review. *Front. Bioeng. Biotechnol.* **2022**, *10*, 973297. [[CrossRef](#)]
119. Shao, H.; Zhang, Q.; Sun, M.; Wu, M.; Sun, X.; Wang, Q.; Tong, S. Effects of hydroxyapatite-coated porous titanium scaffolds functionalized by exosomes on the regeneration and repair of irregular bone. *Front. Bioeng. Biotechnol.* **2023**, *11*, 1283811. [[CrossRef](#)]
120. Frazier, W.E. Metal Additive Manufacturing: A Review. *J. Mater. Eng. Perform.* **2014**, *23*, 1917–1928. [[CrossRef](#)]
121. Nadagouda, M.N.; Rastogi, V.; Ginn, M. A review on 3D printing techniques for medical applications. *Curr. Opin. Chem. Eng.* **2020**, *28*, 152–157. [[CrossRef](#)]
122. Yang, G.; Liu, H.; Li, A.; Liu, T.; Lu, Q.; He, F. Antibacterial Structure Design of Porous Ti6Al4V by 3D Printing and Anodic Oxidation. *Materials* **2023**, *16*, 5206. [[CrossRef](#)]
123. Sun, X.; Tong, S.; Yang, S.; Guo, S. The Effects of Graphene on the Biocompatibility of a 3D-Printed Porous Titanium Alloy. *Coatings* **2021**, *11*, 1509. [[CrossRef](#)]
124. Wang, C.; Yu, D. Comparison of electron beam melting fabrication of irregularity porous Ti-6Al-4V and Ti-24Nb-4Zr-8Sn titanium alloy Scaffolds: Cytocompatibility and osteogenesis. *Clin. Oral Implant. Res.* **2020**, *31*, 110. [[CrossRef](#)]
125. Kuryło, P.; Cykowska-Błasik, M.; Tertel, E.; Pałka, Ł.; Pruszyński, P.; Klekiel, T. Novel Development of Implant Elements Manufactured through Selective Laser Melting 3D Printing. *Adv. Eng. Mater.* **2021**, *23*, 2001488. [[CrossRef](#)]
126. Okazaki, Y.; Nishimura, E.; Nakada, H.; Kobayashi, K. Surface analysis of Ti-15Zr-4Nb-4Ta alloy after implantation in rat tibia. *Biomaterials* **2001**, *22*, 599–607. [[CrossRef](#)]
127. Kazantseva, N.V.; Krakhmalev, P.V.; Yadroitsava, I.A.; Yadroitsev, I.A. Laser Additive 3D Printing of Titanium Alloys: Current Status, Problems, Trends. *Phys. Met. Metallogr.* **2021**, *122*, 6–25. [[CrossRef](#)]

128. Montufar, E.B.; Tkachenko, S.; Casas-Luna, M.; Škarvada, P.; Slámečka, K.; Diaz-de-la-Torre, S.; Koutný, D.; Paloušek, D.; Koledova, Z.; Hernández-Tapia, L.; et al. Benchmarking of additive manufacturing technologies for commercially-pure-titanium bone-tissue-engineering scaffolds: Processing-microstructure-property relationship. *Addit. Manuf.* **2020**, *36*, 101516. [[CrossRef](#)]
129. Yasin, M.S.; Soltani-Tehrani, A.; Shao, S.; Haghshenas, M.; Shamsaei, N. A Comparative Study on Fatigue Performance of Various Additively Manufactured Titanium Alloys. *Procedia Struct. Integr.* **2022**, *38*, 519–525. [[CrossRef](#)]
130. Gao, Y.; Lalevéé, J.; Simon-Masseron, A. An Overview on 3D Printing of Structured Porous Materials and Their Applications. *Adv. Mater. Technol.* **2023**, *8*, 2300377. [[CrossRef](#)]
131. Zheng, Y.; Han, Q.; Wang, J.; Li, D.; Song, Z.; Yu, J. Promotion of Osseointegration between Implant and Bone Interface by Titanium Alloy Porous Scaffolds Prepared by 3D Printing. *ACS Biomater. Sci. Eng.* **2020**, *6*, 5181–5190. [[CrossRef](#)]
132. Zhao, L.; Pei, X.; Jiang, L.; Hu, C.; Sun, J.; Xing, F.; Zhou, C.; Fan, Y.; Zhang, X. Bionic design and 3D printing of porous titanium alloy scaffolds for bone tissue repair. *Compos. Part B Eng.* **2019**, *162*, 154–161. [[CrossRef](#)]
133. Mani, N.; Sola, A.; Trinchi, A.; Fox, K. Is there a future for additive manufactured titanium bioglass composites in biomedical application? A perspective. *Biointerphases* **2020**, *15*, 068501. [[CrossRef](#)]
134. Xu, W.; Zhang, B.; Addison, O.; Wang, X.; Hou, B.; Yu, F. Mechanically-assisted crevice corrosion and its effect on materials degradation. *Corros. Commun.* **2023**, *11*, 23–32. [[CrossRef](#)]
135. Geringer, J.; Pellier, J.; Taylor, M.L.; Macdonald, D.D. Electrochemical Impedance Spectroscopy: Insights for fretting corrosion experiments. *Tribol. Int.* **2013**, *68*, 67–76. [[CrossRef](#)]
136. Rodrigues, D.C.; Urban, R.M.; Jacobs, J.J.; Gilbert, J.L. In vivo severe corrosion and hydrogen embrittlement of retrieved modular body titanium alloy hip-implants. *J. Biomed. Mater. Res. Part B Appl. Biomater.* **2009**, *88B*, 206–219. [[CrossRef](#)]
137. Witt, F.; Bosker, B.H.; Bishop, N.E.; Ettema, H.B.; Verheyen, C.C.P.M.; Morlock, M.M. The Relation between Titanium Taper Corrosion and Cobalt-Chromium Bearing Wear in Large-Head Metal-on-Metal Total Hip Prostheses: A Retrieval Study. *JBJS* **2014**, *96*, e157. [[CrossRef](#)]
138. Vieira, A.C.; Ribeiro, A.R.; Rocha, L.A.; Celis, J.P. Influence of pH and corrosion inhibitors on the tribocorrosion of titanium in artificial saliva. *Wear* **2006**, *261*, 994–1001. [[CrossRef](#)]
139. Mehkri, S.; Abishek, N.R.; Sumanth, K.S.; Rekha, N. Study of the Tribocorrosion occurring at the implant and implant alloy Interface: Dental implant materials. *Mater. Today Proc.* **2021**, *44*, 157–165. [[CrossRef](#)]
140. Alves, S.A.; Beline, T.; Barão, V.A.R.; Sukotjo, C.; Mathew, M.T.; Rocha, L.A.; Celis, J.P.; Souza, J.C.M. Chapter 3—Degradation of titanium-based implants. In *Nanostructured Biomaterials for Cranio-Maxillofacial and Oral Applications*; Souza, J.C.M., Hotza, D., Henriques, B., Boccaccini, A.R., Eds.; Elsevier: Amsterdam, The Netherlands, 2018; pp. 41–62.
141. Chaturvedi, T.P. An overview of the corrosion aspect of dental implants (titanium and its alloys). *Indian J. Dent. Res. Off. Publ. Indian Soc. Dent. Res.* **2009**, *20*, 91–98. [[CrossRef](#)]
142. Han, X.; Ma, J.; Tian, A.; Wang, Y.; Li, Y.; Dong, B.; Tong, X.; Ma, X. Surface modification techniques of titanium and titanium alloys for biomedical orthopaedics applications: A review. *Colloids Surf. B Biointerfaces* **2023**, *227*, 113339. [[CrossRef](#)]
143. Makurat-Kasprolewicz, B.; Ossowska, A. Recent advances in electrochemically surface treated titanium and its alloys for biomedical applications: A review of anodic and plasma electrolytic oxidation methods. *Mater. Today Commun.* **2023**, *34*, 105425. [[CrossRef](#)]
144. Costa, T.N.Q.; Dotta, T.C.; Galo, R.; Soares, M.E.d.C.; Pedrazzi, V. Effect of tribocorrosion on surface-treated titanium alloy implants: A systematic review with meta-analysis. *J. Mech. Behav. Biomed. Mater.* **2023**, *145*, 106008. [[CrossRef](#)] [[PubMed](#)]
145. Unune, D.R.; Brown, G.R.; Reilly, G.C. Thermal based surface modification techniques for enhancing the corrosion and wear resistance of metallic implants: A review. *Vacuum* **2022**, *203*, 111298. [[CrossRef](#)]
146. Bai, H.; Zhong, L.; Kang, L.; Liu, J.; Zhuang, W.; Lv, Z.; Xu, Y. A review on wear-resistant coating with high hardness and high toughness on the surface of titanium alloy. *J. Alloys Compd.* **2021**, *882*, 160645. [[CrossRef](#)]
147. Fu, Y.; Zhou, F.; Wang, Q.; Zhang, M.; Zhou, Z. Electrochemical and tribocorrosion performances of CrMoSiCN coating on Ti-6Al-4V titanium alloy in artificial seawater. *Corros. Sci.* **2020**, *165*, 108385. [[CrossRef](#)]
148. Hatem, A.; Lin, J.; Wei, R.; Torres, R.D.; Laurindo, C.; de Souza, G.B.; Soares, P. Tribocorrosion behavior of low friction TiSiCN nanocomposite coatings deposited on titanium alloy for biomedical applications. *Surf. Coat. Technol.* **2018**, *347*, 1–12. [[CrossRef](#)]
149. Mendizabal, L.; Lopez, A.; Bayón, R.; Herrero-Fernandez, P.; Barriga, J.; Gonzalez, J.J. Tribocorrosion response in biological environments of multilayer TaN films deposited by HPPMS. *Surf. Coat. Technol.* **2016**, *295*, 60–69. [[CrossRef](#)]
150. Grabarczyk, J.; Gaj, J.; Pazik, B.; Kaczorowski, W.; Januszewicz, B. Tribocorrosion behavior of Ti6Al4V alloy after thermo-chemical treatment and DLC deposition for biomedical applications. *Tribol. Int.* **2021**, *153*, 106560. [[CrossRef](#)]
151. Manhobosco, T.M.; Tamborim, S.M.; dos Santos, C.B.; Müller, I.L. Tribological, electrochemical and tribo-electrochemical characterization of bare and nitrided Ti6Al4V in simulated body fluid solution. *Corros. Sci.* **2011**, *53*, 1786–1793. [[CrossRef](#)]
152. Rahmatian, B.; Ghasemi, H.M.; Heydarzadeh Sohi, M.; De Baets, P. Tribocorrosion and corrosion behavior of double borided layers formed on Ti-6Al-4V alloy: An approach for applications to bio-implants. *Corros. Sci.* **2023**, *210*, 110824. [[CrossRef](#)]
153. Cheng, K.-y.; Pagan, N.; Bijukumar, D.; Mathew, M.T.; McNallan, M. Carburized titanium as a solid lubricant on hip implants: Corrosion, tribocorrosion and biocompatibility aspects. *Thin Solid Film.* **2018**, *665*, 148–158. [[CrossRef](#)]
154. Li, K.M.; Song, K.J.; Guan, J.; Yang, F.; Liu, J. Tribocorrosion behavior of a Ti6Al4V alloy electromagnetic induction nitride layer in a fluorine-containing solution. *Surf. Coat. Technol.* **2020**, *386*, 125506. [[CrossRef](#)]

155. Çaha, I.; Alves, A.C.; Affonço, L.J.; Lisboa-Filho, P.N.; da Silva, J.H.D.; Rocha, L.A.; Pinto, A.M.P.; Toptan, F. Corrosion and tribocorrosion behaviour of titanium nitride thin films grown on titanium under different deposition times. *Surf. Coat. Technol.* **2019**, *374*, 878–888. [[CrossRef](#)]
156. Bayón, R.; Igartua, A.; González, J.J.; Ruiz de Gopegui, U. Influence of the carbon content on the corrosion and tribocorrosion performance of Ti-DLC coatings for biomedical alloys. *Tribol. Int.* **2015**, *88*, 115–125. [[CrossRef](#)]
157. Wang, Y.; Li, J.; Dang, C.; Wang, Y.; Zhu, Y. Influence of carbon contents on the structure and tribocorrosion properties of TiSiCN coatings on Ti6Al4V. *Tribol. Int.* **2017**, *109*, 285–296. [[CrossRef](#)]
158. Zhu, Y.; Dong, M.; Li, J.; Wang, L. The improved corrosion and tribocorrosion properties of TiSiN/Ag by thermal treatment. *Surf. Coat. Technol.* **2020**, *385*, 125437. [[CrossRef](#)]
159. Dong, M.; Zhu, Y.; Xu, L.; Ren, X.; Ma, F.; Mao, F.; Li, J.; Wang, L. Tribocorrosion performance of nano-layered coating in artificial seawater. *Appl. Surf. Sci.* **2019**, *487*, 647–654. [[CrossRef](#)]
160. Fazel, M.; Salimijazi, H.R.; Golozar, M.A. A comparison of corrosion, tribocorrosion and electrochemical impedance properties of pure Ti and Ti6Al4V alloy treated by micro-arc oxidation process. *Appl. Surf. Sci.* **2015**, *324*, 751–756. [[CrossRef](#)]
161. de Viteri, V.S.; Bayón, R.; Igartua, A.; Barandika, G.; Moreno, J.E.; Peremarch, C.P.-J.; Pérez, M.M. Structure, tribocorrosion and biocide characterization of Ca, P and I containing TiO<sub>2</sub> coatings developed by plasma electrolytic oxidation. *Appl. Surf. Sci.* **2016**, *367*, 1–10. [[CrossRef](#)]
162. Zuo, Y.; Li, T.; Yu, P.; Zhao, Z.; Chen, X.; Zhang, Y.; Chen, F. Effect of graphene oxide additive on tribocorrosion behavior of MAO coatings prepared on Ti6Al4V alloy. *Appl. Surf. Sci.* **2019**, *480*, 26–34. [[CrossRef](#)]
163. Zhang, H.; Cui, H.; Man, C.; Liu, F.; Pang, K.; Ma, G.; Chen, H.; Cui, Z. The tribocorrosion resistance of TiN + TiB/TC4 composite coatings and the synergistic strengthening effects of multi-level reinforcements. *Corros. Sci.* **2023**, *219*, 111224. [[CrossRef](#)]
164. Kovács, D.; Quintana, I.; Dobránszky, J. Effects of Different Variants of Plasma Nitriding on the Properties of the Nitrided Layer. *J. Mater. Eng. Perform.* **2019**, *28*, 5485–5493. [[CrossRef](#)]
165. Kertscher, R.; Brunatto, S.F. On the kinetics of nitride and diffusion layer growth in niobium plasma nitriding. *Surf. Coat. Technol.* **2020**, *401*, 126220. [[CrossRef](#)]
166. Miao, B.; Chai, Y.; Wei, K.; Hu, J. A novel duplex plasma treatment combining plasma nitrocarburizing and plasma nitriding. *Vacuum* **2016**, *133*, 54–57. [[CrossRef](#)]
167. Sun, J.; Yao, Q.T.; Zhang, Y.H.; Du, X.D.; Wu, Y.C.; Tong, W.P. Simultaneously improving surface mechanical properties and in vitro biocompatibility of pure titanium via surface mechanical attrition treatment combined with low-temperature plasma nitriding. *Surf. Coat. Technol.* **2017**, *309*, 382–389. [[CrossRef](#)]
168. Yang, W.; He, X.; Li, H.; Dong, J.; Chen, W.; Xin, H.; Jin, Z. A tribological investigation of SLM fabricated TC4 titanium alloy with carburization pre-treatment. *Ceram. Int.* **2020**, *46*, 3043–3050. [[CrossRef](#)]
169. Zhao, Z.; Hui, P.; Wang, T.; Wang, X.; Xu, Y.; Zhong, L.; Zhao, M. New strategy to grow TiC coatings on titanium alloy: Contact solid carburization by cast iron. *J. Alloys Compd.* **2018**, *745*, 637–643. [[CrossRef](#)]
170. Yang, C.; Liu, J. Intermittent vacuum gas nitriding of TB8 titanium alloy. *Vacuum* **2019**, *163*, 52–58. [[CrossRef](#)]
171. Luk'yanenko, A.G.; Pohrelyuk, I.M.; Shlyakhetka, K.S.; Skrebtsov, A.A.; Kravchysyn, T.M. Nitriding of Sintered VT-1-0 Titanium Alloy. *Powder Metall. Met. Ceram.* **2020**, *59*, 249–260. [[CrossRef](#)]
172. Pohrelyuk, I.M.; Tkachuk, O.V.; Proskurnyak, R.V.; Boiko, N.M.; Kluchivska, O.Y.; Stoika, R.S. Effect of Thermodiffusion Nitriding on Cytocompatibility of Ti-6Al-4V Titanium Alloy. *JOM* **2016**, *68*, 1109–1115. [[CrossRef](#)]
173. Sun, H.-z.; Zheng, J.; Song, Y.; Chi, J.; Fu, Y.-d. Effect of the deformation on nitrocarburizing microstructure of the cold deformed Ti-6Al-4V alloy. *Surf. Coat. Technol.* **2019**, *362*, 234–238. [[CrossRef](#)]
174. Darmawan, A.S.; Siswanto, W.A.; Purboputro, P.I.; Febriantoko, B.W.; Sujitno, T.; Hamid, A. Predicting Surface Hardness of Commercially Pure Titanium Under Plasma Nitrocarburizing Based on Experimental Data. *IOP Conf. Ser. Mater. Sci. Eng.* **2020**, *990*, 012022. [[CrossRef](#)]
175. Li, Y.; He, Y.; Wang, W.; Mao, J.; Zhang, L.; Zhu, Y.; Ye, Q. Plasma Nitriding of AISI 304 Stainless Steel in Cathodic and Floating Electric Potential: Influence on Morphology, Chemical Characteristics and Tribological Behavior. *J. Mater. Eng. Perform.* **2018**, *27*, 948–960. [[CrossRef](#)]
176. Zhang, C.; Wen, K.; Gao, Y. Columnar and nanocrystalline combined microstructure of the nitrided layer by active screen plasma nitriding on surface-nanocrystalline titanium alloy. *Appl. Surf. Sci.* **2023**, *617*, 156614. [[CrossRef](#)]
177. Li, Y.; Zhou, Z.; Yi, X.; Yan, J.; Xiu, J.; Fang, D.; Shao, M.; Ren, P.; He, Y.; Qiu, J. Improved seawater corrosion resistance of electron beam melting Ti6Al4V titanium alloy by plasma nitriding. *Vacuum* **2023**, *216*, 112463. [[CrossRef](#)]
178. Wu, J.; Liu, H.; Li, J.; Yang, X.; Hu, J. Comparative study of plasma oxynitriding and plasma nitriding for AISI 4140 steel. *J. Alloys Compd.* **2016**, *680*, 642–645. [[CrossRef](#)]
179. Fernandes, F.A.P.; Heck, S.C.; Picone, C.A.; Casteletti, L.C. On the wear and corrosion of plasma nitrided AISI H13. *Surf. Coat. Technol.* **2020**, *381*, 125216. [[CrossRef](#)]
180. Wang, X.; Bai, S.; Li, F.; Li, D.; Zhang, J.; Tian, M.; Zhang, Q.; Tong, Y.; Zhang, Z.; Wang, G.; et al. Effect of plasma nitriding and titanium nitride coating on the corrosion resistance of titanium. *J. Prosthet. Dent.* **2016**, *116*, 450–456. [[CrossRef](#)]
181. Li, Y.; He, Y.; Zhang, S.; Wang, W.; Zhu, Y. Microstructure and corrosion resistance of nitrogen-rich surface layers on AISI 304 stainless steel by rapid nitriding in a hollow cathode discharge. *Appl. Phys. A* **2017**, *124*, 65. [[CrossRef](#)]

182. Wang, C.; Huang, H.; Wu, H.; Hong, J.; Zhang, L.; Yan, J. Ultra-low wear of titanium alloy surface under lubricated conditions achieved by laser texturing and simultaneous nitriding. *Surf. Coat. Technol.* **2023**, *474*, 130083. [[CrossRef](#)]
183. Li, Y.; Zhou, Z.; He, Y. Solid Lubrication System and Its Plasma Surface Engineering: A Review. *Lubricants* **2023**, *11*, 473. [[CrossRef](#)]
184. Yan, J.; Shao, M.; Zhou, Z.; Zhang, Z.; Yi, X.; Wang, M.; Xie, B.; He, Y.; Li, Y. Electrochemical Corrosion Behavior of Ti-N-O Modified Layer on the TC4 Titanium Alloy Prepared by Hollow Cathodic Plasma Source Oxynitriding. *Metals* **2023**, *13*, 1083. [[CrossRef](#)]
185. Li, Y.; Wang, Z.; Shao, M.; Zhang, Z.; Wang, C.; Yan, J.; Lu, J.; Zhang, L.; Xie, B.; He, Y.; et al. Characterization and electrochemical behavior of a multilayer-structured Ti-N layer produced by plasma nitriding of electron beam melting TC4 alloy in Hank's solution. *Vacuum* **2023**, *208*, 111737. [[CrossRef](#)]
186. Liu, J.; Wang, X.; Hu, Y.; Luo, L.; Jiang, C.; Liu, F.; Jin, W.; Zhu, K.; Long, Z.; Liu, K. Effect of hydrogen on microstructure and mechanical properties of plasma-nitrided pure titanium by cathodic cage plasma nitriding. *Surf. Coat. Technol.* **2023**, *456*, 129231. [[CrossRef](#)]
187. Braz, J.K.F.S.; Martins, G.M.; Morales, N.; Naulin, P.; Fuentes, C.; Barrera, N.P.; Vitoriano, J.O.; Rocha, H.A.O.; Oliveira, M.F.; Alves, C.; et al. Live endothelial cells on plasma-nitrided and oxidized titanium: An approach for evaluating biocompatibility. *Mater. Sci. Eng. C* **2020**, *113*, 111014. [[CrossRef](#)] [[PubMed](#)]
188. El-Hossary, F.M.; Negm, N.Z.; Abd El-Rahman, A.M.; Raaif, M.; Seleem, A.A.; Abd El-Moula, A.A. Tribo-mechanical and electrochemical properties of plasma nitriding titanium. *Surf. Coat. Technol.* **2015**, *276*, 658–667. [[CrossRef](#)]
189. She, D.; Yue, W.; Fu, Z.; Wang, C.; Yang, X.; Liu, J. Effects of nitriding temperature on microstructures and vacuum tribological properties of plasma-nitrided titanium. *Surf. Coat. Technol.* **2015**, *264*, 32–40. [[CrossRef](#)]
190. Zhang, L.; Shao, M.; Zhang, Z.; Yi, X.; Yan, J.; Zhou, Z.; Fang, D.; He, Y.; Li, Y. Corrosion Behavior of Nitrided Layer of Ti6Al4V Titanium Alloy by Hollow Cathodic Plasma Source Nitriding. *Materials* **2023**, *16*, 2961. [[CrossRef](#)]
191. Fujita, K.; Ijiri, M.; Inoue, Y.; Kikuchi, S. Rapid Nitriding of Titanium Alloy with Fine Grains at Room Temperature. *Adv. Mater.* **2021**, *33*, 2008298. [[CrossRef](#)]
192. Chen, Z.; Wang, Z.; Liu, J.; Ye, Z.; Hu, Y.; Wu, J.; Liu, K.; Cai, Z. Enhancing the tribological properties of TA1 pure titanium by modulating the energy of pulsed laser nitriding. *Opt. Laser Technol.* **2024**, *169*, 110118. [[CrossRef](#)]
193. Zhao, G.-H.; Aune, R.E.; Espallargas, N. Tribocorrosion studies of metallic biomaterials: The effect of plasma nitriding and DLC surface modifications. *J. Mech. Behav. Biomed. Mater.* **2016**, *63*, 100–114. [[CrossRef](#)] [[PubMed](#)]
194. Guan, J.; Jiang, X.; Xiang, Q.; Yang, F.; Liu, J. Corrosion and tribocorrosion behavior of titanium surfaces designed by electromagnetic induction nitriding for biomedical applications. *Surf. Coat. Technol.* **2021**, *409*, 126844. [[CrossRef](#)]
195. Fan, W.; Wang, Q.; Yan, Y.; Li, X. Distinctive performance evolution of surface layer in TC4 alloy oxidized at high temperature: Softening or hardening? *J. Alloys Compd.* **2023**, *968*, 172125. [[CrossRef](#)]
196. Zhang, Y.; Ma, G.-R.; Zhang, X.-C.; Li, S.; Tu, S.-T. Thermal oxidation of Ti-6Al-4V alloy and pure titanium under external bending strain: Experiment and modelling. *Corros. Sci.* **2017**, *122*, 61–73. [[CrossRef](#)]
197. Wang, S.; Liu, Y.; Zhang, C.; Liao, Z.; Liu, W. The improvement of wettability, biotribological behavior and corrosion resistance of titanium alloy pretreated by thermal oxidation. *Tribol. Int.* **2014**, *79*, 174–182. [[CrossRef](#)]
198. Januszewicz, B.; Siniarski, D. The glow discharge plasma influence on the oxide layer and diffusion zone formation during process of thermal oxidation of titanium and its alloys. *Vacuum* **2006**, *81*, 215–220. [[CrossRef](#)]
199. Bailey, R.; Sun, Y. Corrosion and Tribocorrosion Performance of Thermally Oxidized Commercially Pure Titanium in a 0.9% NaCl Solution. *J. Mater. Eng. Perform.* **2015**, *24*, 1669–1678. [[CrossRef](#)]
200. Cheraghali, B.; Ghasemi, H.M.; Abedini, M.; Yazdi, R. Functionally graded oxygen-containing coating on CP-titanium for bio-applications: Characterization, biocompatibility and tribocorrosion behavior. *J. Mater. Res. Technol.* **2022**, *21*, 104–120. [[CrossRef](#)]
201. Si, Y.; Liu, H.; Yu, H.; Jiang, X.; Sun, D. A heterogeneous TiO<sub>2</sub>/SrTiO<sub>3</sub> coating on titanium alloy with excellent photocatalytic antibacterial, osteogenesis and tribocorrosion properties. *Surf. Coat. Technol.* **2022**, *431*, 128008. [[CrossRef](#)]
202. Wang, J.; Zhang, M.; Dai, S.; Zhu, L. Research Progress in Electrospark Deposition Coatings on Titanium Alloy Surfaces: A Short Review. *Coatings* **2023**, *13*, 1473. [[CrossRef](#)]
203. Fattah-alhosseini, A.; Molaie, M.; Nouri, M.; Babaei, K. Review of the role of graphene and its derivatives in enhancing the performance of plasma electrolytic oxidation coatings on titanium and its alloys. *Appl. Surf. Sci. Adv.* **2021**, *6*, 100140. [[CrossRef](#)]
204. Li, G.; Ma, F.; Liu, P.; Qi, S.; Li, W.; Zhang, K.; Chen, X. Review of micro-arc oxidation of titanium alloys: Mechanism, properties and applications. *J. Alloys Compd.* **2023**, *948*, 169773. [[CrossRef](#)]
205. Nikoomezari, E.; Karbasi, M.; Melo, W.C.; Moris, H.; Babaei, K.; Giannakis, S.; Fattah-alhosseini, A. Impressive strides in antibacterial performance amelioration of Ti-based implants via plasma electrolytic oxidation (PEO): A review of the recent advancements. *Chem. Eng. J.* **2022**, *441*, 136003. [[CrossRef](#)]
206. Moga, S.; Malinowski, V.; Marin, A.; Coaca, E.; Negrea, D.; Craciun, V.; Lungu, M. Mechanical and corrosion-resistant coatings prepared on AZ63 Mg alloy by plasma electrolytic oxidation. *Surf. Coat. Technol.* **2023**, *462*, 129464. [[CrossRef](#)]
207. Ji, R.; Wang, S.; Zou, Y.; Chen, G.; Wang, Y.; Ouyang, J.; Jia, D.; Zhou, Y. One-step fabrication of amorphous/ITO-CNTs coating by plasma electrolytic oxidation with particle addition for excellent wear resistance. *Appl. Surf. Sci.* **2023**, *640*, 158274. [[CrossRef](#)]

208. Lukiyanchuk, I.V.; Tarkhanova, I.G.; Vasilyeva, M.S.; Yarovaya, T.P.; Ustinov, A.Y.; Vyalyi, I.E.; Kuryavyi, V.G. Plasma electrolytic formation of TiO<sub>2</sub>-VO<sub>x</sub>-MoO<sub>y</sub>-P<sub>2</sub>O<sub>5</sub> coatings on titanium and their application as catalysts for the oxidation of S- and N-containing substances. *Mater. Chem. Phys.* **2024**, *311*, 128520. [\[CrossRef\]](#)
209. Maciej, A.; Marny, M.; Sowa, M.; Blacha-Grzechnik, A.; Stolarczyk, A.; Michalska, J.; Simka, W. Microstructure and corrosion resistance of Ti and Ti-40Nb alloy modified by plasma electrolytic oxidation in tricalcium phosphate suspension. *Electrochim. Acta* **2023**, *468*, 143185. [\[CrossRef\]](#)
210. White, L.; Koo, Y.; Neralla, S.; Sankar, J.; Yun, Y. Enhanced mechanical properties and increased corrosion resistance of a biodegradable magnesium alloy by plasma electrolytic oxidation (PEO). *Mater. Sci. Eng. B* **2016**, *208*, 39–46. [\[CrossRef\]](#)
211. Farhadi, S.S.; Aliofkhaezrai, M.; Barati Darband, G.; Abolhasani, A.; Sabour Rouhaghdam, A. Wettability and Corrosion Behavior of Chemically Modified Plasma Electrolytic Oxidation Nanocomposite Coating. *J. Mater. Eng. Perform.* **2017**, *26*, 4797–4806. [\[CrossRef\]](#)
212. Yavari, S.A.; Necula, B.S.; Fratila-Apachitei, L.E.; Duszczuk, J.; Apachitei, I. Biofunctional surfaces by plasma electrolytic oxidation on titanium biomedical alloys. *Surf. Eng.* **2016**, *32*, 411–417. [\[CrossRef\]](#)
213. Guo, Z.; Yang, Z.; Chen, Y.; Li, H.; Zhao, Q.; Xu, Y.; Zhan, H.; Hao, J.; Zhao, Y. One-step plasma electrolytic oxidation with Graphene oxide for Ultra-low porosity Corrosion-resistant TiO<sub>2</sub> coatings. *Appl. Surf. Sci.* **2022**, *594*, 153477. [\[CrossRef\]](#)
214. Yu, X.; Chen, L.; Qin, H.; Wu, M.; Yan, Z. Formation process of in situ oxide coatings with high porosity using one-step plasma electrolytic oxidation. *Appl. Surf. Sci.* **2016**, *366*, 432–438. [\[CrossRef\]](#)
215. Alves, S.A.; Bayón, R.; Igartua, A.; Saénz de Viteri, V.; Rocha, L.A. Tribocorrosion behaviour of anodic titanium oxide films produced by plasma electrolytic oxidation for dental implants. *Lubr. Sci.* **2014**, *26*, 500–513. [\[CrossRef\]](#)
216. Laurindo, C.A.H.; Bembem, L.M.; Torres, R.D.; Mali, S.A.; Gilbert, J.L.; Soares, P. Influence of the annealing treatment on the tribocorrosion properties of Ca and P containing TiO<sub>2</sub> produced by plasma electrolytic oxidation. *Mater. Technol.* **2016**, *31*, 719–725. [\[CrossRef\]](#)
217. Sukuroglu, E.E.; Farzi, H.; Sukuroglu, S.; Totik, Y.; Arslan, E.; Efeoglu, I. The effect of plasma electrolytic oxidation process parameters on the tribocorrosion properties of TiO<sub>2</sub> coatings. *J. Adhes. Sci. Technol.* **2017**, *31*, 1361–1373. [\[CrossRef\]](#)
218. He, B.; Xin, C.; Chen, Y.; Xu, Y.; Zhao, Q.; Hou, Z.; Tang, Y.; Liu, H.; Su, X.; Zhao, Y. Biological performance and tribocorrosion behavior of in-situ synthesized CuxO/TiO<sub>2</sub> coatings. *Appl. Surf. Sci.* **2022**, *600*, 154096. [\[CrossRef\]](#)
219. Krella, A. Resistance of PVD Coatings to Erosive and Wear Processes: A Review. *Coatings* **2020**, *10*, 921. [\[CrossRef\]](#)
220. Baptista, A.; Silva, F.; Porteiro, J.; Míguez, J.; Pinto, G. Sputtering Physical Vapour Deposition (PVD) Coatings: A Critical Review on Process Improvement and Market Trend Demands. *Coatings* **2018**, *8*, 402. [\[CrossRef\]](#)
221. Inspektor, A.; Salvador, P.A. Architecture of PVD coatings for metalcutting applications: A review. *Surf. Coat. Technol.* **2014**, *257*, 138–153. [\[CrossRef\]](#)
222. Baptista, A.; Silva, F.J.G.; Porteiro, J.; Míguez, J.L.; Pinto, G.; Fernandes, L. On the Physical Vapour Deposition (PVD): Evolution of Magnetron Sputtering Processes for Industrial Applications. *Procedia Manuf.* **2018**, *17*, 746–757. [\[CrossRef\]](#)
223. Oskirko, V.O.; Goncharenko, I.M.; Arestov, S.I.; Semenov, V.A.; Azhgikhin, M.I.; Pavlov, A.P.; Solovyev, A.A. Short pulse-enhanced vacuum arc evaporation. *Vacuum* **2022**, *205*, 111459. [\[CrossRef\]](#)
224. Staszuk, M.; Pakuła, D.; Chladek, G.; Pawlyta, M.; Pancielejko, M.; Czaja, P. Investigation of the structure and properties of PVD coatings and ALD + PVD hybrid coatings deposited on sialon tool ceramics. *Vacuum* **2018**, *154*, 272–284. [\[CrossRef\]](#)
225. Bobzin, K.; Brögelmann, T.; Gillner, A.; Kruppe, N.C.; He, C.; Naderi, M. Laser-structured high performance PVD coatings. *Surf. Coat. Technol.* **2018**, *352*, 302–312. [\[CrossRef\]](#)
226. Bobzin, K.; Kalscheuer, C.; Möbius, M.P. Triboactive CrAlN + MoWS coatings deposited by pulsed arc PVD. *Surf. Coat. Technol.* **2023**, *475*, 130178. [\[CrossRef\]](#)
227. Bobzin, K.; Kalscheuer, C.; Carlet, M.; Schulze, C. From cathode to substrate: Plasma diagnostics on high power pulsed magnetron sputtering deposition of titanium nitride. *Thin Solid Film.* **2022**, *755*, 139331. [\[CrossRef\]](#)
228. Bai, X.; Xu, L.; Shi, X.; Ren, J.; Xu, L.; Wang, Q.; Li, B.; Liu, Z.; Zheng, C.; Fu, Q. Hydrothermal oxidation improves corrosion and wear properties of multi-arc ion plated titanium nitride coating for biological application. *Vacuum* **2022**, *198*, 110871. [\[CrossRef\]](#)
229. Bello, M.; Shanmugan, S. Achievements in mid and high-temperature selective absorber coatings by physical vapor deposition (PVD) for solar thermal Application—A review. *J. Alloys Compd.* **2020**, *839*, 155510. [\[CrossRef\]](#)
230. Vorobyova, M.; Biffoli, F.; Giurlani, W.; Martinuzzi, S.M.; Linsler, M.; Caneschi, A.; Innocenti, M. PVD for Decorative Applications: A Review. *Materials* **2023**, *16*, 4919. [\[CrossRef\]](#)
231. Navinšek, B. Improvement of cutting tools by TiN PVD hard coating. *Mater. Manuf. Process.* **1992**, *7*, 363–382. [\[CrossRef\]](#)
232. Sathish, M.; Radhika, N.; Saleh, B. A critical review on functionally graded coatings: Methods, properties, and challenges. *Compos. Part B Eng.* **2021**, *225*, 109278. [\[CrossRef\]](#)
233. Huang, X.; Xie, Z.; Li, K.; Chen, Q.; Gong, F.; Chen, Y.; Feng, B.; Hu, S.; Chen, Y.; Han, B.; et al. Microstructure, wear and oxidation resistance of CrWN glass molding coatings synthesized by plasma enhanced magnetron sputtering. *Vacuum* **2020**, *174*, 109206. [\[CrossRef\]](#)
234. Xie, Q.; Sun, G.; Fu, Z.; Kang, J.; Zhu, L.; She, D.; Lin, S. Comparative study of titanium carbide films deposited by plasma-enhanced and conventional magnetron sputtering at various methane flow rates. *Ceram. Int.* **2023**, *49*, 25269–25282. [\[CrossRef\]](#)

235. Zhang, X.; Zhou, Y.-W.; Gao, J.-B.; Zhao, Z.-W.; Guo, Y.-Y.; Xie, Z.-W.; Kelly, P. Effect of the filament discharge current on the microstructure and performance of plasma-enhanced magnetron sputtered TiN coatings. *J. Alloys Compd.* **2017**, *725*, 877–883. [[CrossRef](#)]
236. El-Rahman, A.M.A.; Wei, R. A comparative study of conventional magnetron sputter deposited and plasma enhanced magnetron sputter deposited Ti–Si–C–N nanocomposite coatings. *Surf. Coat. Technol.* **2014**, *241*, 74–79. [[CrossRef](#)]
237. Choi, Y.H.; Huh, J.Y.; Baik, Y.J. Radial microstructural nonuniformity of boron nitride films deposited on a wafer scale substrate by unbalanced magnetron sputtering. *Thin Solid Film.* **2023**, *769*, 139753. [[CrossRef](#)]
238. Rosaz, G.; Bartkowska, A.; Carlos, C.P.A.; Richard, T.; Taborelli, M. Niobium thin film thickness profile tailoring on complex shape substrates using unbalanced biased High Power Impulse Magnetron Sputtering. *Surf. Coat. Technol.* **2022**, *436*, 128306. [[CrossRef](#)]
239. Wang, T.; Zhang, Q.; Yu, S.; Zhang, G. Development of latent fingerprints by unbalanced magnetron sputtering deposited ultra-thin metal film. *Vacuum* **2021**, *194*, 110577. [[CrossRef](#)]
240. Shanker, G.; Prathap, P.; Srivatsa, K.M.K.; Singh, P. Effect of balanced and unbalanced magnetron sputtering processes on the properties of SnO<sub>2</sub> thin films. *Curr. Appl. Phys.* **2019**, *19*, 697–703. [[CrossRef](#)]
241. Fu, Y.; Zhou, F.; Zhang, M.; Wang, Q.; Zhou, Z. Structural, mechanical and tribocorrosion performances of CrMoSiN coatings with various Mo contents in artificial seawater. *Appl. Surf. Sci.* **2020**, *525*, 146629. [[CrossRef](#)]
242. Challali, F.; Touam, T.; Bockelée, V.; Chauveau, T.; Chelouche, A.; Stephant, N.; Hamon, J.; Besland, M.-P. Comprehensive characterization of Al-doped ZnO thin films deposited in confocal radio frequency magnetron co-sputtering. *Thin Solid Film.* **2023**, *780*, 139947. [[CrossRef](#)]
243. Aliasghari, S.; Avcu, E.; Skeldon, P.; Valizadeh, R.; Mingo, B. Abrasion resistance of a Nb<sub>3</sub>Sn magnetron-sputtered coating on copper substrates for radio frequency superconducting cavities. *Mater. Des.* **2023**, *231*, 112030. [[CrossRef](#)]
244. Mian, M.S.; Nakano, T.; Okimura, K. Improvement of the uniformity of structural and electrical properties of transparent conductive Al-doped ZnO thin films by inductively coupled plasma-assisted radio frequency magnetron sputtering. *Thin Solid Film.* **2023**, *769*, 139752. [[CrossRef](#)]
245. Stan, G.E.; Montazerian, M.; Shearer, A.; Stuart, B.W.; Baino, F.; Mauro, J.C.; Ferreira, J.M.F. Critical Advances in the Field of Magnetron Sputtered Bioactive Glass Thin-Films: An Analytical Review. *Appl. Surf. Sci.* **2023**, *646*, 158760. [[CrossRef](#)]
246. Yang, T.; Zhang, Z.; Song, S.; Li, Y.; Lv, M.; Wu, Z.; Han, S. Structural, optical and electrical properties of AZO/Cu/AZO tri-layer films prepared by radio frequency magnetron sputtering and ion-beam sputtering. *Vacuum* **2008**, *83*, 257–260. [[CrossRef](#)]
247. Zhao, C.; Zhu, Y.; Yuan, Z.; Li, J. Structure and tribocorrosion behavior of Ti/TiN multilayer coatings in simulated body fluid by arc ion plating. *Surf. Coat. Technol.* **2020**, *403*, 126399. [[CrossRef](#)]
248. Cai, F.; Zhou, Q.; Chen, J.; Zhang, S. Effect of inserting the Zr layers on the tribo-corrosion behavior of Zr/ZrN multilayer coatings on titanium alloys. *Corros. Sci.* **2023**, *213*, 111002. [[CrossRef](#)]
249. Behzadi, P.; Badr, M.; Zakeri, A. Duplex surface modification of pure Ti via thermal oxidation and gas nitriding: Preparation and electrochemical studies. *Ceram. Int.* **2022**, *48*, 34374–34381. [[CrossRef](#)]
250. Kim, J.-I.; Lee, W.-Y.; Tokoroyama, T.; Umehara, N. Long-term low-friction of Ti-overcoated and-doped DLCs: Robustly developed carbonous transfer layer with titanium. *Carbon* **2023**, *204*, 268–283. [[CrossRef](#)]
251. Łepicka, M.; Građzka-Dahlke, M.; Zaborowska, I.; Górski, G.; Mosdorf, R. Recurrence analysis of coefficient of friction oscillations in DLC-coated and non-coated Ti6Al4V titanium alloy. *Tribol. Int.* **2022**, *165*, 107342. [[CrossRef](#)]
252. Dhandapani, V.S.; Kang, K.-M.; Seo, K.-J.; Kim, C.-L.; Kim, D.-E. Enhancement of tribological properties of DLC by incorporation of amorphous titanium using magnetron sputtering process. *Ceram. Int.* **2019**, *45*, 11971–11981. [[CrossRef](#)]
253. Bharathy, P.V.; Nataraj, D.; Chu, P.K.; Wang, H.; Yang, Q.; Kiran, M.S.R.N.; Silvestre-Albero, J.; Mangalaraj, D. Effect of titanium incorporation on the structural, mechanical and biocompatible properties of DLC thin films prepared by reactive-biased target ion beam deposition method. *Appl. Surf. Sci.* **2010**, *257*, 143–150. [[CrossRef](#)]
254. Xu, Y.R.; Liu, H.D.; Chen, Y.M.; Yousaf, M.I.; Luo, C.; Wan, Q.; Hu, L.W.; Fu, D.J.; Ren, F.; Li, Z.G.; et al. In situ synthesized TiC–DLC nanocomposite coatings on titanium surface in acetylene ambient. *Appl. Surf. Sci.* **2015**, *349*, 93–100. [[CrossRef](#)]
255. Hinüber, C.; Kleemann, C.; Friederichs, R.J.; Haubold, L.; Scheibe, H.J.; Schuelke, T.; Boehlert, C.; Baumann, M.J. Biocompatibility and mechanical properties of diamond-like coatings on cobalt-chromium-molybdenum steel and titanium-aluminum-vanadium biomedical alloys. *J. Biomed. Mater. Res. Part A* **2010**, *95A*, 388–400. [[CrossRef](#)] [[PubMed](#)]
256. Arslan, E.; Totik, Y.; Efeoglu, I. The investigation of the tribocorrosion properties of DLC coatings deposited on Ti6Al4V alloys by CFUBMS. *Prog. Org. Coat.* **2012**, *74*, 768–771. [[CrossRef](#)]
257. Manhabosco, T.M.; Müller, I.L. Tribocorrosion of Diamond-Like Carbon Deposited on Ti6Al4V. *Tribol. Lett.* **2009**, *34*, 229. [[CrossRef](#)]
258. Sankar Kumar, A.; Jeeva, P.A.; Karthikeyan, S. Evaluation of wear resistance and microstructural properties of laser clad martensitic and austenitic stainless steel. *Mater. Today Proc.* **2023**, *in press*. [[CrossRef](#)]
259. Yang, H.; Shi, M.; Zhao, E.; Wang, Q.; Liu, H.; Hao, J. Microstructure evolution of laser clad NiCrBSi coating assisted by an in-situ laser shock wave. *J. Mater. Process. Technol.* **2023**, *321*, 118132. [[CrossRef](#)]
260. Li, R.; Feng, A.; Zhao, J.; Pan, X.; Zhang, G.; Zhu, Y.; Chen, C. Study on process optimization of WC–Ni60A cermet composite coating by laser cladding. *Mater. Today Commun.* **2023**, *37*, 107400. [[CrossRef](#)]

261. Mohsan, A.U.H.; Zhang, M.; Wang, D.; Zhao, S.; Wang, Y.; Chen, C.; Zhang, J. State-of-the-art review on the Ultrasonic Vibration Assisted Laser Cladding (UVALC). *J. Manuf. Process.* **2023**, *107*, 422–446. [[CrossRef](#)]
262. Sypniewska, J.; Szkodo, M. Influence of Laser Modification on the Surface Character of Biomaterials: Titanium and Its Alloys—A Review. *Coatings* **2022**, *12*, 1371.
263. Deng, C.; Yi, Y.; Jiang, M.; Hu, L.; Zhou, S. Microstructure and high-temperature resistance of Al<sub>2</sub>O<sub>3</sub>/CoNiCrAlY coatings by laser cladding. *Ceram. Int.* **2023**, *49*, 32885–32895. [[CrossRef](#)]
264. Ding, H.; Cao, Y.; Hua, K.; Tong, Y.; Li, N.; Sun, L.; Li, X.; Wu, H.; Wang, H. Fretting wear resistance at ambient and elevated temperatures of 316 stainless steel improved by laser cladding with Co-based alloy/WC/CaF<sub>2</sub> composite coating. *Opt. Laser Technol.* **2023**, *163*, 109428. [[CrossRef](#)]
265. Wan, S.; Cui, X.; Liu, K.; Jin, G.; Wang, S.; Zhao, Y.; Li, J.; Yang, Y.; Guan, Y. Preparation of AlTiVN/Cu/Cu–Al gradient functional coating via laser cladding for enhanced wear and corrosion resistance of MgLi alloy. *Surf. Coat. Technol.* **2023**, *475*, 130137. [[CrossRef](#)]
266. Zhao, T.; Wang, L.; Zhang, S.; Zhang, C.H.; Sun, X.Y.; Chen, H.T.; Bai, X.L.; Wu, C.L. Effect of synergistic cavitation erosion-corrosion on cavitation damage of CoCrFeNiMn high entropy alloy layer by laser cladding. *Surf. Coat. Technol.* **2023**, *472*, 129940. [[CrossRef](#)]
267. Ding, H.; Yang, T.; Wang, W.; Zhu, Y.; Lin, Q.; Guo, J.; Xiao, Q.; Gan, L.; Liu, Q. Optimization and wear behaviors of 316L stainless steel laser cladding on rail material. *Wear* **2023**, *523*, 204830. [[CrossRef](#)]
268. Ouyang, C.; Wang, R.; Zhao, C.; Wei, R.; Li, H.; Deng, R.; Bai, Q.; Liu, Y. Multi-layer laser cladding analysis and high-temperature oxidative wear behavior of cast iron with a low expansion coefficient. *Surf. Coat. Technol.* **2023**, *474*, 130079. [[CrossRef](#)]
269. Obadele, B.A.; Andrews, A.; Olubambi, P.A.; Mathew, M.T.; Pityana, S. Tribocorrosion behaviour of laser clad biomedical grade titanium alloy. *Mater. Corros.* **2015**, *66*, 1133–1139. [[CrossRef](#)]
270. Zammit, A.; Attard, M.; Subramaniyan, P.; Levin, S.; Wagner, L.; Cooper, J.; Espitalier, L.; Cassar, G. Enhancing surface integrity of titanium alloy through hybrid surface modification (HSM) treatments. *Mater. Chem. Phys.* **2022**, *279*, 125768. [[CrossRef](#)]
271. Sypniewska, J.; Szkodo, M.; Majkowska-Marzec, B.; Mielewczyk-Gryń, A. Effect of hybrid modification by ceramic layer formation in MAO process and laser remelting on the structure of titanium bio-alloy Ti13Nb13Zr. *Ceram. Int.* **2023**, *49*, 16603–16614. [[CrossRef](#)]
272. Yang, Z.; Xu, W.; Zhang, W.; Chen, Y.; Shan, D. Effect of power spinning and heat treatment on microstructure evolution and mechanical properties of duplex low-cost titanium alloy. *J. Mater. Sci. Technol.* **2023**, *136*, 121–139. [[CrossRef](#)]
273. Czyrska-Filemonowicz, A.; Buffat, P.A.; Wierzchon, T. Microstructure and properties of hard layers formed by duplex surface treatment containing nickel and phosphorus on a titanium-base alloy. *Scr. Mater.* **2005**, *53*, 1439–1442. [[CrossRef](#)]
274. Hamrahi, B.; Yarmand, B.; Massoudi, A. Improved in-vitro corrosion performance of titanium using a duplex system of plasma electrolytic oxidation and graphene oxide incorporated silane coatings. *Surf. Coat. Technol.* **2021**, *422*, 127558. [[CrossRef](#)]
275. Padilha Fontoura, C.; Ló Bertele, P.; Machado Rodrigues, M.; Elisa Dotta Maddalozzo, A.; Frassini, R.; Silvestrin Celi Garcia, C.; Tomaz Martins, S.; Crespo, J.d.S.; Figueroa, C.A.; Roesch-Ely, M.; et al. Comparative Study of Physicochemical Properties and Biocompatibility (L929 and MG63 Cells) of TiN Coatings Obtained by Plasma Nitriding and Thin Film Deposition. *ACS Biomater. Sci. Eng.* **2021**, *7*, 3683–3695. [[CrossRef](#)] [[PubMed](#)]
276. Cheraghali, B.; Ghasemi, H.M.; Abedini, M.; Yazdi, R. A functionalized duplex coating on CP-titanium for biomedical applications. *Surf. Coat. Technol.* **2020**, *399*, 126117. [[CrossRef](#)]
277. ASTM F2129; Standard Test Method for Conducting Cyclic Potentiodynamic Polarization Measurements to Determine the Corrosion Susceptibility of Small Implant Devices. ASTM International: West Conshohocken, PA, USA, 2019.
278. Esfahani, E.A.; Bukuaghangin, O.; Banfield, S.; Vangölü, Y.; Yang, L.; Neville, A.; Hall, R.; Bryant, M. Surface engineering of wrought and additive layer manufactured Ti-6Al-4V alloy for enhanced load bearing and bio-tribocorrosion applications. *Surf. Coat. Technol.* **2022**, *442*, 128139. [[CrossRef](#)]
279. Dong, M.; Zhu, Y.; Wang, C.; Shan, L.; Li, J. Structure and tribocorrosion properties of duplex treatment coatings of TiSiCN/nitride on Ti6Al4V alloy. *Ceram. Int.* **2019**, *45*, 12461–12468. [[CrossRef](#)]
280. Zhao, C.; Gao, W.; Wang, J.; Ju, J.; Li, J. A novel biomedical TiN-embedded TiO<sub>2</sub> nanotubes composite coating with remarkable mechanical properties, corrosion, tribocorrosion resistance, and antibacterial activity. *Ceram. Int.* **2023**, *49*, 15629–15640. [[CrossRef](#)]
281. Kao, W.H.; Su, Y.L.; Hsieh, Y.T. Effects of Duplex Nitriding and TiN Coating Treatment on Wear Resistance, Corrosion Resistance and Biocompatibility of Ti6Al4V Alloy. *J. Mater. Eng. Perform.* **2017**, *26*, 3686–3697. [[CrossRef](#)]
282. Vella, K.A.; Buhagiar, J.; Cassar, G.; Pizzuto, M.M.; Bonnici, L.; Chen, J.; Zhang, X.; Huang, Z.; Zammit, A. The Effect of a Duplex Surface Treatment on the Corrosion and Tribocorrosion Characteristics of Additively Manufactured Ti-6Al-4V. *Materials* **2023**, *16*, 2098. [[CrossRef](#)]
283. Zhang, Y.; Chen, F.; Zhang, Y.; Liu, M.; Pang, Y.; Du, C. Enhanced corrosion and tribocorrosion properties of duplex TiN-MAO coating prepared on TC17 alloys. *Surf. Coat. Technol.* **2022**, *444*, 128662. [[CrossRef](#)]
284. Hatem, A.; Lin, J.; Wei, R.; Torres, R.D.; Laurindo, C.; Soares, P. Tribocorrosion behavior of DLC-coated Ti-6Al-4V alloy deposited by PIID and PEMS+PIID techniques for biomedical applications. *Surf. Coat. Technol.* **2017**, *332*, 223–232. [[CrossRef](#)]



- 
285. Wei, R. Development of new technologies and practical applications of plasma immersion ion deposition (PIID). *Surf. Coat. Technol.* **2010**, *204*, 2869–2874. [[CrossRef](#)]
286. Kong, W.; Li, K.; Hu, J. TEM Structure, Nanomechanical Property, and Adhesive Force of Magnetron-Sputtered Cr-DLC Coating on a Nitrided Ti6Al4V Alloy. *J. Phys. Chem. C* **2021**, *125*, 16733–16745.

**Disclaimer/Publisher’s Note:** The statements, opinions and data contained in all publications are solely those of the individual author(s) and contributor(s) and not of MDPI and/or the editor(s). MDPI and/or the editor(s) disclaim responsibility for any injury to people or property resulting from any ideas, methods, instructions or products referred to in the content.